

Drew University  
College of the Liberal Arts

**Carbon Isotope Discrimination in *Ginkgo*: Testing A Paleo-CO<sub>2</sub> Proxy**

A Thesis in Chemistry

By

Mason Scher

Submitted in Partial Fulfillment  
Of the Requirements  
For the Degree of  
Bachelor in Arts  
With Specialized Honors in Chemistry

May 2020

### *Acknowledgements*

I can attribute the richness of my undergraduate experience to my professors, mentors, friends, and family. My family encouraged my interests in the outdoors and science since I was very young, and has always been the most wonderful support system. When I came to Drew, Dr. Mary-Ann Pearsall and Dr. Ryan Hinrichs quickly became two of my most important mentors. My freshman year, Dr. Hinrichs trusted me in his research lab and gave me (what I thought was far too much) freedom during DSSI, but made me confident in the lab and research thereafter. Dr. Pearsall has been a constant source of advice, reality checks, and support through college. I can't thank Dr. Eickmeyer enough for uttering the word that changed my life, "paleoclimatology," in the RISE Science Seminar my freshman year. When I started thinking about pursuing geoscience and paleoclimate, all three of these mentors pushed me towards opportunities in and outside of Drew to explore geoscience. One of these opportunities came in the form of an REU in the Paleobiology Department at the Smithsonian Institution NMNH, where I was introduced to Dr. Scott Wing and Dr. Rich Barclay in the summer of 2018. Their willingness to let me make decisions and spend many hours a week thinking through ideas and teaching me solidified my interest in geoscience.

I'd like to give thanks to the interns that I've worked with at NMNH and SERC over the past two summers, Ian Handler, James Sappington, Lily Bennet, and Alex Kane, as well as all of the wonderful Fossil Atmospheres volunteers who made this project possible (special thanks to Linda Davidson!). Allie Baczynski saved my data collection in the summer of 2018, and I am deeply indebted to her. My friends have been my home,

safety net, and major source of motivation at Drew. Thank you to Saif Yasin, Zoe Coates, Hunter Muratore, and Samantha Keegan.

### *Table of Contents*

Acknowledgements.....	2
Abstract.....	4
Chapter One: Introduction .....	6
Case Study.....	6
Current Climate Change and the Need for Paleoclimate Reconstructions.....	8
Paleoclimate Proxies.....	13
The C3 Plant Proxy.....	19
Chapter Two: Materials and Methods .....	27
Chapter Three: Results.....	41
Chapter Four: Discussion.....	50
Chapter Five: Conclusion.....	68
Works Cited.....	69

### ***Abstract***

Anthropogenic climate change poses a major threat to our current way of life. Without understanding how earth systems will react to growing anthropogenic CO<sub>2</sub> emissions, it is impossible to properly plan. Reconstructions of CO<sub>2</sub> levels (paleo-CO<sub>2</sub>) and other important environmental parameters from the geologic past give a long-term record of earth system changes which are invaluable for understanding just how sensitive earth systems are. While there are several methods of reconstructing paleo-CO<sub>2</sub>, more are needed to corroborate existing reconstructions and to fill in important gaps in time. The Paleocene-Eocene Thermal Maximum (PETM) was a transient warm peak about 56 million years ago and is the best analog of future climate change. Paleo-CO<sub>2</sub> reconstructions are lacking during this important event, preventing an understanding of how much atmospheric CO<sub>2</sub> gave rise to the 5-8°C temperature increase of the PETM. *Ginkgo* has been used widely to reconstruct CO<sub>2</sub> levels in the geological past because living *Ginkgo biloba* closely resembles common Mesozoic and Paleogene fossils of the genus. Many *Ginkgo* fossils from around the time of the PETM have been collected, and would be useful for paleo-CO<sub>2</sub> reconstructions. Atmospheric CO<sub>2</sub> levels in the geological past have been inferred from the  $\delta^{13}\text{C}$  of plant fossils following experimental evidence in *Arabidopsis* and *Raphanus*, where leaf-level discrimination against <sup>13</sup>C ( $\Delta^{13}\text{C}$ , or difference between  $\delta^{13}\text{C}$  of atmosphere and leaf) was found to increase with *p*CO<sub>2</sub>. Higher *p*CO<sub>2</sub> leads to higher CO<sub>2</sub> within the leaf (*C*<sub>i</sub>), allowing RuBisCO to more strongly discriminate against <sup>13</sup>C. *Ginkgo* has been used widely to reconstruct CO<sub>2</sub> levels in the geological past because living *Ginkgo biloba* closely resembles common Mesozoic and Paleogene fossils of the genus. We therefore constructed an experiment to test if



$\Delta^{13}\text{C}$  in *Ginkgo* was positively correlated with  $p\text{CO}_2$ . For four years (2016-2019) we grew *Ginkgo biloba* trees outdoors in open-topped chambers under ambient light and temperature fluctuations but with  $\text{CO}_2$  levels of  $\sim 400$ ,  $\sim 600$ ,  $\sim 800$ , and  $\sim 1000$  ppm (three trees at each  $\text{CO}_2$  level). Data from the 2018 and 2019 growing season gave an unexpected relationship between  $p\text{CO}_2$  and  $\Delta^{13}\text{C}$  where  $\Delta^{13}\text{C}$  has a slightly negative relationship with  $p\text{CO}_2$ . Our work shows that the relationship between  $\Delta^{13}\text{C}$  and  $p\text{CO}_2$  is not the same in *Ginkgo* as in *Arabidopsis* and *Raphanus*. A compilation of studies of  $\Delta^{13}\text{C}$  in a variety of species shows no consistent relationship to be used as a paleo- $\text{CO}_2$  proxy. If the relationship of  $\Delta^{13}\text{C}$  to  $p\text{CO}_2$  varies among taxa, caution should be taken in reconstructing ancient  $\text{CO}_2$  concentrations from  $\Delta^{13}\text{C}$  of mixed fossil organic matter or molecular fossils. Further work with physiological data from this experiment may show that stomatal regulation prevents  $C_i$  from increasing with increasing  $p\text{CO}_2$ , which would prevent  $\Delta^{13}\text{C}$  from increasing with increasing  $p\text{CO}_2$ .

## *Introduction*

### *Case Study – The Paleocene-Eocene Thermal Maximum*

During the late Paleocene, 56 million years ago, a large but unquantified amount of carbon was released into the earth's atmosphere. Before this quick change (less than 20,000 years), the present-day Bighorn Basin in Wyoming was covered by a diverse forest ecosystem, rich with flora and fauna. This changed dramatically with a sharp increase in atmospheric carbon dioxide (Figure 1) and temperature increase of 5-8°C [McInerney and Wing 2011]. The forest of the Bighorn Basin turned to an arid shrubland, and mammal species in the area changed as heat-intolerant species migrated north and others moved in. After ~100,000 years of this thermal maximum, the ecosystem recovered to pre-event rainfall, flora, and fauna over a period of ~100,000 years. This rapid environmental change is known as the Paleocene Eocene Thermal Maximum, or PETM. It is the closest analog of climate change and carbon input for the current changes we are seeing in our environment. The rapidity with which the PETM occurred is unmatched in geologic history; other warm periods like the Early Eocene Climatic Optimum (or EECO) lasted over 4.1 million years [Westerhold et al. 2018]. The study of the PETM is of great importance for understanding how earth reacts to sudden increases in atmospheric carbon and recovers over time.

The actual amount of carbon added to the atmosphere during the PETM is unfortunately poorly constrained. In sediments, both marine and terrestrial, the PETM is demarcated by a carbon isotope excursion (CIE), meaning that less  $^{13}\text{C}$  was found relative to  $^{12}\text{C}$  in carbonate rocks, microfossil shells, and fossil teeth [McInerney and Wing 2011]. This global decrease resulted from release of  $^{12}\text{C}$  enriched carbon at the onset of the

PETM, which then circulated through the atmosphere and ocean. There are several theories for where this light carbon came from: methane clathrates, wildfires, thermogenic methane, drying seaways, and permafrost thawing, or more likely some combination. Each of these potential sources has a known isotopic signature. Mass balance calculations have been used to model the amount of carbon coming from each source that would be required to give the PETM CIE. The relative amounts of carbon from each source must combine to create the same isotopic value as the observed CIE. Unfortunately, mass balance calculations for the amount of carbon released do not agree with other models of PETM carbon release [Zeebe et al. 2009; Panchuk et al. 2008], so estimates of  $p\text{CO}_2$  for the PETM range from 700 to 25,000 ppm  $\text{CO}_2$ , an enormous spread [McInerney and Wing 2011]. Without well-constrained estimates of  $p\text{CO}_2$  for the PETM, matching extreme environmental change with atmospheric  $p\text{CO}_2$  is fraught with assumptions and error. With reliable estimates of  $p\text{CO}_2$  for the PETM, climate sensitivity for this period can be calculated and the source(s) of carbon input for the onset of the PETM will be better constrained.

Aside from models and mass-balance calculations that attempt to estimate  $p\text{CO}_2$ , information stored in the geologic record can give estimates. Current geologic  $p\text{CO}_2$  data are few and far between, lacking the resolution to see the transient PETM and evaluate the height of  $p\text{CO}_2$ . Better resolution of this data and/or new methods of using this data are needed to aid the study of the PETM.



**Figure 1.** Reconstruction of the Bighorn Basin, Wyoming before, during, and after the PETM. Before the PETM, this area had a warm and wet climate, with conifers and water-tolerant species. During the body of the PETM, the area became warmer and dry, losing much of the species present before. After the PETM, vegetation was similar to the pre-PETM. Art by Aldo Chiappe, for National Geographic.

### ***Section One: Current Climate Change and the Need for Paleoclimate Reconstructions***

In this section, modern global climate change and the greenhouse effect are briefly described. The need for paleoclimate reconstructions and better-constrained paleoclimate proxies are explained, as they inform our understanding of how climate will continue to change.

Global climate change has taken more of the world stage as we begin to see real change happening and threatening the comfortable, carefree manner in which we consume. Extreme heat, variable rainfall, and ease of spreading infection are on the rise. World Health Organization (WHO) estimates that between 2030 and 2050, an additional 250,000 deaths per year will be a result of climate change, and the cost of damage to health will be between 2 and 4 billion dollars [IPCC 2014]. Climate change is something we all must take seriously, and not just for the distant future, but for the very near future

and even the present. Having a complete understanding of climate is important for being able to predict future changes and prepare accordingly.

While climate changes naturally, the culprit for these modern global changes is largely anthropogenic gases released into the atmosphere, the most common of which are CO<sub>2</sub>, CH<sub>4</sub>, and N<sub>2</sub>O [IPCC 2014]. When solar radiation hits the earth's surface (as UV and visible light which travels easily through the atmosphere) it is absorbed. This is then re-emitted as infrared radiation and exits the atmosphere, if it is not trapped before escaping by gases like CO<sub>2</sub> and CH<sub>4</sub>. Infrared radiation causes the C-O and C-H bonds in these gases to vibrate, increasing their kinetic energy and turning infrared radiation into heat. This is what is called the "Greenhouse Effect". As the concentration of these greenhouse gases (GHG's) increases in the atmosphere, more infrared radiation is converted to heat, and global temperatures continue to rise.

Before industrialization (~1850), global carbon dioxide levels were at 280 ppm. In May of 2019, the observatory at Mauna Loa recorded a concentration of 414.7 ppm, a whopping 3.5 ppm higher than May just the year before [NOAA] (Figure 2). If emissions continue at the current rate, *p*CO<sub>2</sub> could reach >1000 ppm by 2100 [IPCC 2018]. A level of >1000 ppm would be unprecedented, considering that for the last 650,000 years, *p*CO<sub>2</sub> fluctuated between 180 to 300 ppm (Figure 3) through glacial (cold) and interglacial (warm) periods [IPCC 2013].

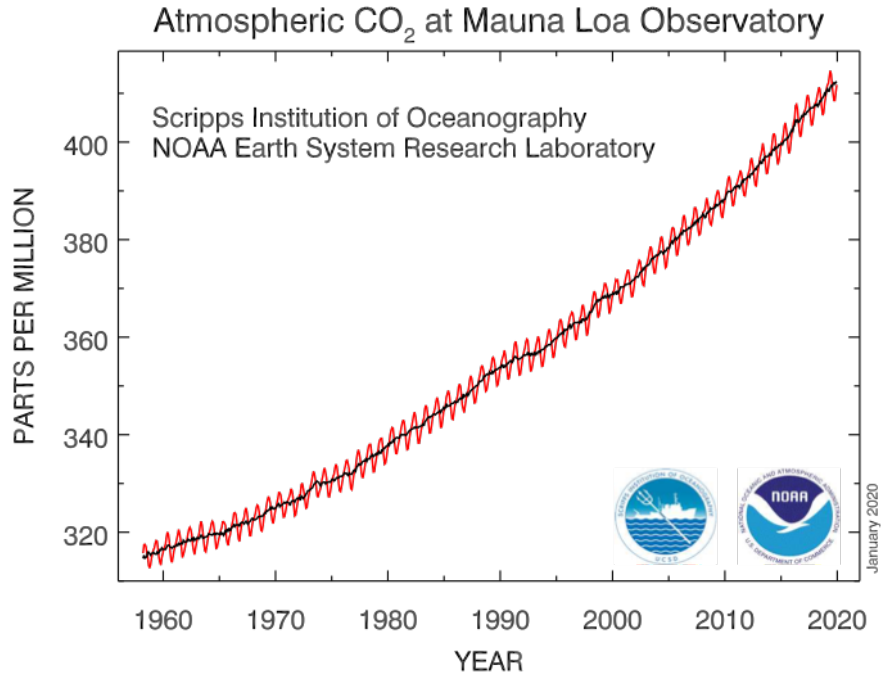


**Figure 2.** The record of  $p\text{CO}_2$  recorded at Hawaii’s Mauna Loa Observatory. This observatory has been recording atmospheric  $p\text{CO}_2$  since 1958. The red line shows the monthly average  $p\text{CO}_2$ , and the cyclic nature is due to seasonal  $\text{CO}_2$  changes. The black line is corrected for those changes using a 7-pt moving average [NOAA].

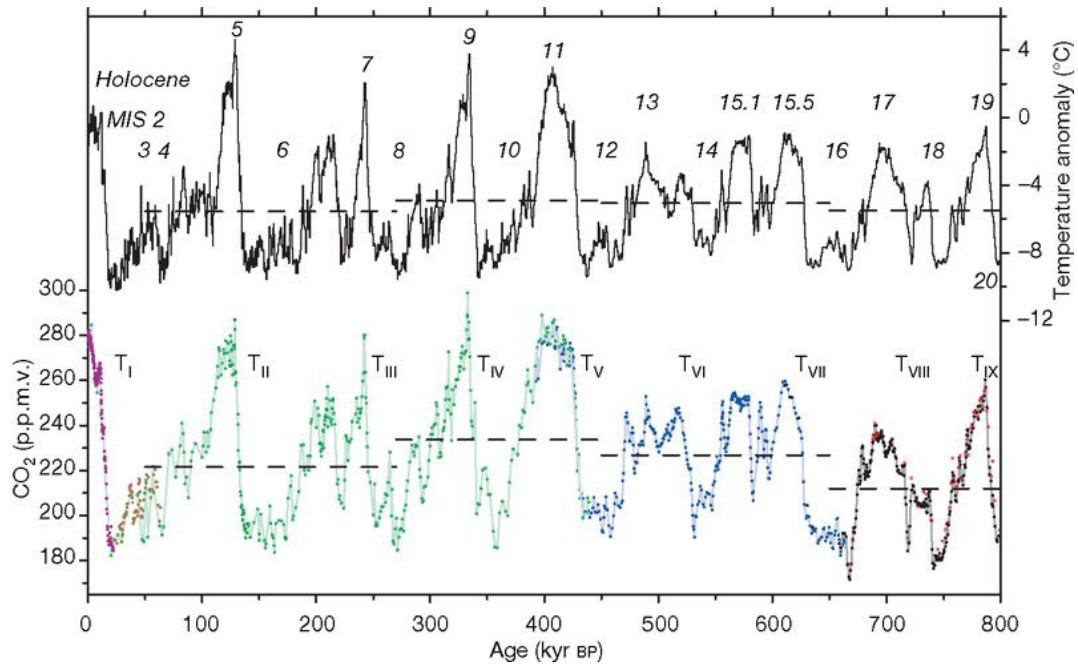


**Figure 3.** Figure 2 in Lüthi et al. 2008.  $p\text{CO}_2$  and temperature record through the last 800,00 years from Antarctic ice cores. Colors represent different cores. T with subscript represents the end of glacial periods, and numbers represent Marine Isotope Stages (MIS).

The most recent IPCC special report stated that current warming from anthropogenic emissions has reached  $1^\circ\text{C}$ . In order to limit global warming to  $1.5^\circ\text{C}$ , greenhouse emissions would have to be net zero by 2055 at the latest [IPCC 2018]. These estimates are dependent upon our understanding of climate sensitivity, or how affected the earth is by changes in  $p\text{CO}_2$ . High climate sensitivity would mean that the earth would warm a lot from a small change in  $p\text{CO}_2$ , while low climate sensitivity would give a small change in temperature with a small change in  $p\text{CO}_2$ .

It is hard to understand climate sensitivity on short timescales like pre-industrialization to now. This modern period has the advantage of being well-documented, but we are unable to know if there are lags in certain earth processes that will manifest in the next 100 or more years as a result of increasing  $p\text{CO}_2$ . Studying the earth in this limited window of time simply does not give enough data. If we reduce emissions to net zero by 2055 (as is needed to stay under  $1.5^\circ\text{C}$  increase in global temperature), we cannot be sure how long it will take for the earth to recover back to pre-industrial temperatures or  $\text{CO}_2$  levels. Climate data on longer timescales are necessary to project how our climate will change in the future.

To aid in this understanding of longer processes, the study of past environmental and climatic changes in earth (geologic) history are necessary. Paleoclimatology relies on material and information being recorded in the geologic record that can be accessed today using the tools of geology, chemistry, physics, and biology. When these data are used to

infer environmental conditions, it is called a paleoclimate proxy. A proxy is the geologically preserved material used to reconstruct environmental conditions, and the relationship between this material and variables in the environment/climate. Proxies can be applied to the geologic record to reconstruct precipitation, temperature,  $p\text{CO}_2$ , ocean pH, magnetic reversals, trophic level, and weathering, to name some. Using proxies, climate can be reconstructed over geologic history: 10s or 100s of millions of years. These longer time slices enable paleoclimatologists to look at climate sensitivity on long scales with differing  $p\text{CO}_2$  levels and track how temperature, sea levels, and other variables change with  $p\text{CO}_2$ .

These paleoclimate reconstructions provide information for climate models. Climate models are built with knowledge about how the earth functions today and how we know that it has functioned in the past from paleoclimate reconstructions and studies. Additionally, paleoclimate reconstructions act as test data sets for these models. From reconstructions, scientists know what happened before and after a certain time in the geologic record (so long as the proxy data is well understood). Modelers can use the “before” data as inputs for their climate model, and compare the outputs of the model to what is known about the “after” from paleoclimate reconstructions. If the models are in good agreement with the paleoclimate data, then the model is working. If the model and the paleoclimate data are not in good agreement, then the model needs to be revised.

With the rapid changes that people are causing to the planet, it is of utmost importance to continue studying our earth in the geologic record. While much is known about past changes, many reconstructions are poorly constrained.  $p\text{CO}_2$  reconstructions



are unfortunately especially fraught and require much more work to get estimates with much less error. These problems will be discussed in the next section.

### ***Paleoclimate Proxies***

In section one, the need for paleoclimate reconstructions and proxies was explained. In section two, a variety of proxies will be briefly described, and several  $p\text{CO}_2$  proxies will be described more in depth.

Some proxies are more direct than others. Ice cores are an example of a fairly direct proxy for  $\text{CO}_2$ . These cores contain bubbles of air from when ice formed, giving nearly direct measurements of  $\text{CO}_2$  levels (when snow accumulation rate, diffusion, and other factors are accounted for). Less direct proxies are more numerous and give information that is calibrated to phenomena (temperature,  $p\text{CO}_2$ , rainfall, etc.) in the climate, requiring additional studies to connect the proxy to the phenomena of interest through proxy development and calibration. Proxy methods rely on an understanding of biological, chemical, geological, and physical processes and an assumption that these processes have not changed over time. The types of proxies are sometimes broken up into three categories: biological, physical, and chemical proxies.

Biological proxies depend on the preservation of biological material, in the form of fossils or organic matter. Aside from chemical studies that can be performed on fossils, a number of climate reconstructions can be created from morphology and assemblages. In assemblage studies, plant macrofossils are used to characterize the environment of a period by the types of plant fossils that are found in a certain area during a certain time.

Assemblages of plant fossils have been collected and studied before, during, and after the PETM in the Bighorn Basin. Wing and Currano [2013] found extreme floral changes surrounding the PETM. Water-tolerant species and conifers were common both before and after the PETM, but within the PETM were almost completely absent. During the body of the PETM, drought-tolerant species like legumes became dominant. The drastic change in plant assemblages shows that before and after the PETM, the Bighorn Basin region was cooler and wetter as compared to the hot and dry body of the PETM. This change had to be drastic enough to lead to the extirpation of 88% of species present during the late Paleocene [Wing and Currano, 2013].

Physical proxies utilize properties of deposited sediments, like grain size, color, texture, or magnetic alignment to say something about the environment. The size of particles deposited during a certain period in a certain location tells you about the energy of the water moving through the area: high-energy water will deposit large rocks and sediments, and low-energy water may only deposit silt. The color of paleosols, or geologically preserved soils, can tell a great deal about paleoenvironments. The color is indicative of the minerals formed within the preserved soils: red indicates the presence of hematite, forming when wet soil gets dried out, and purple paleosols contain much less hematite, indicating less drying of soil. In the Bighorn Basin, paleosols formed before the PETM are purple and represent a period of poorly drained soil. At the onset of the PETM, the paleosols were much better drained and red, and during the body of the PETM the paleosols are largely yellow and filled with carbonate nodules (calcium carbonate filling in burrows) indicating very good draining. These paleosols tell a story of a wet climate

before the PETM and a dry climate during the PETM. During the recovery of the PETM, red paleosols formed, and purple paleosols after recovery [Kraus et al. 2013].

Chemical proxies can be applied to a number of materials: soils, fossils, rocks, etc. One example of a chemical proxy is the use of oxygen isotopes to reconstruct temperature/global ice volume. Many of the basic concepts used in this proxy are also an important part of the work in this study, so I'll take some time to explain delta notation ( $\delta$ ) and how delta values are calculated here.

Oxygen exists in three stable isotopes:  $^{16}\text{O}$  is the dominant isotope, and has an average abundance on earth of 99.76%.  $^{18}\text{O}$  has an average abundance of 0.2%, and  $^{17}\text{O}$  0.04%. Variations in the  $^{18}\text{O}/^{16}\text{O}$  isotopic composition of materials can provide information linked to environmental and geologic processes.  $^{17}\text{O}$  is generally too low in abundance to make meaningful measurements, though some researchers can make high-precision measurements. For simplicity,  $^{17}\text{O}$  will be ignored in this discussion.

Measurements of  $^{18}\text{O}$  and  $^{16}\text{O}$  in a sample are expressed as  $\delta^{18}\text{O}$ , following equation 1:

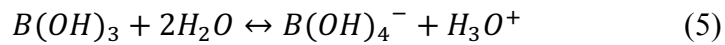
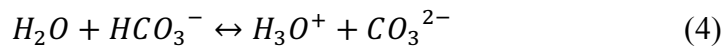
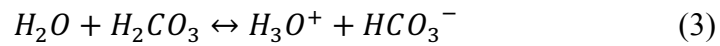
$$\delta^{18}\text{O} (\text{‰}) = \left( \frac{(^{18}\text{O}/^{16}\text{O})_{\text{sample}}}{(^{18}\text{O}/^{16}\text{O})_{\text{standard}}} - 1 \right) * 1000 \quad (1)$$

$^{18}\text{O}/^{16}\text{O}$  ratios are measured using isotope ratio mass spectrometers. For every isotope system, there is a standard (or standards) that samples are referenced against. In the case of  $\delta^{18}\text{O}$ , that standard is usually Standard Mean Ocean Water, or SMOW.  $\delta$  values are expressed in units ‰, permille, or part per thousand. A high value of  $\delta^{18}\text{O}$  means that there is a lot of  $^{18}\text{O}$  in the sample, the sample is enriched in  $^{18}\text{O}$ . A low value means there is very little  $^{18}\text{O}$  in the sample, the sample is depleted in  $^{18}\text{O}$ .

When water evaporates from the surface of the ocean, it contains both  $\text{H}_2^{18}\text{O}$  and  $\text{H}_2^{16}\text{O}$ . As this air mass containing water vapor lifts via convection and travels to higher latitudes, it cools. Following a Rayleigh fractionation process, the heavier  $\text{H}_2^{18}\text{O}$  condenses and rains out more readily than the  $\text{H}_2^{16}\text{O}$ , so the  $\delta^{18}\text{O}$  of the remaining water vapor becomes lower (depleted in the heavy  $\text{H}_2^{18}\text{O}$ ). By the time this water vapor precipitates over land, it is extremely depleted in  $^{18}\text{O}$ . During a warm period of climate, this precipitation would likely make its way back to the ocean. During cold climates, however, this precipitation falls as snow or ice which does not melt. Frozen water continues to accumulate on land, enriched in  $^{16}\text{O}$ . As water continues to evaporate from the ocean and deposit  $^{16}\text{O}$  on land in the form of snow and ice, the ocean becomes increasingly enriched in  $^{18}\text{O}$ . The change in  $\delta^{18}\text{O}$  of the ocean is recorded in the calcium carbonate ( $\text{CaCO}_3$ ) shells of tiny plankton called foraminifera which they precipitate from sea water. The  $\delta^{18}\text{O}$  value of these shells also, however, records temperature as the fractionation between  $^{18}\text{O}$  and  $^{16}\text{O}$  during precipitation of  $\text{CaCO}_3$  is temperature dependent [Emiliani 1955]. These components can be separated with a few tricks, and foraminifera are able to give record of both global ice volume and ocean temperature, though more work is needed to refine this distinction [Marchitto 2014].

Isotopes are used in a variety of other ways for paleoclimate reconstructions as well, all relying on fractionation processes that are recorded in the rock record. For example, the ratio of the stable isotopes of boron ( $^{11}\text{B}/^{10}\text{B}$ ) preserved in corals and the shells of foraminifera are related to the pH of the ocean at the time that the shells or coral formed. This paleo-pH reconstruction can further be related to atmospheric  $\text{CO}_2$  as ocean acidification is a result of atmospheric  $\text{CO}_2$  entering the ocean, forming carbonic acid,

and driving down the pH, following Equations 2-4. Change in pH causes the equilibrium between boric acid ( $B(OH)_3$ ) and the borate ( $B(OH)_4^-$ ) ion to shift (Equation 5).  $^{10}B$  preferentially exists in the borate ion, but under more acidic conditions,  $^{11}B$  residing in boric acid is converted to borate, which is incorporated into the shells of foraminifera. The higher the ratio of  $^{11}B/^{10}B$  in these shells, the lower the ocean pH and the higher the atmospheric concentration of  $CO_2$  [Zeebe 2005; Klochko et al. 2006].



Paleo- $CO_2$  proxies like the boron proxy have been developed, but are problematic. The world's oldest ice core, discovered just in October of 2019, is 2.7 million years old [Voosen 2019]. This means that the oldest direct proxy of  $pCO_2$ , the air bubbles traced in this ice, can only go back that far, 2.7 million years. Indirect proxies for  $pCO_2$  include the boron proxy mentioned above [Zeebe 2004; Klochko et al. 2006], paleosol measurements of carbon isotopes in calcite and goethite [Cotton and Sheldon 2012], carbon isotopes in phytoplankton and bryophytes [Freeman and Hayes 1992; Fletcher et al. 2005], plant stomatal measurements [Royer 2001], carbon isotopes of cave deposits (speleothems) [Wong and Breecker 2015], and one direct (but rarely found) evaporite mineral called Nahcolite ( $NaHCO_3$ ) which only precipitates above 680 ppm  $CO_2$  and directly incorporates atmospheric carbon [Jagniecki et al. 2015].

Nahcolite is unfortunately very rare, so these paleo-CO<sub>2</sub> reconstructions are hard to come by. The boron proxy, and carbon isotope measurements in phytoplankton, bryophytes, speleothems, and paleosols are all subject to error in estimates arising from an incomplete understanding of the fractionation steps that result in the final isotopic composition in the material. Stomatal measurements have recently been reevaluated [Barclay and Wing 2016], and *p*CO<sub>2</sub> reconstructions in deep time are forthcoming. In addition to refining and calibrating current paleo-CO<sub>2</sub> proxy methods, more ought to be developed. With an increase in the types of proxies and records that are created from these proxies, the signal to noise ratio increases. From Figure 4 [IPCC 2013], it is clear that the further back we go into the geologic record, uncertainty increases dramatically (blue shaded area). Not only is variability high, but reconstructions in periods of particular interest, like the PETM 56 Ma, are few and far between. A high-resolution record of paleo-CO<sub>2</sub> reconstructions is necessary to catch this transient warm peak.

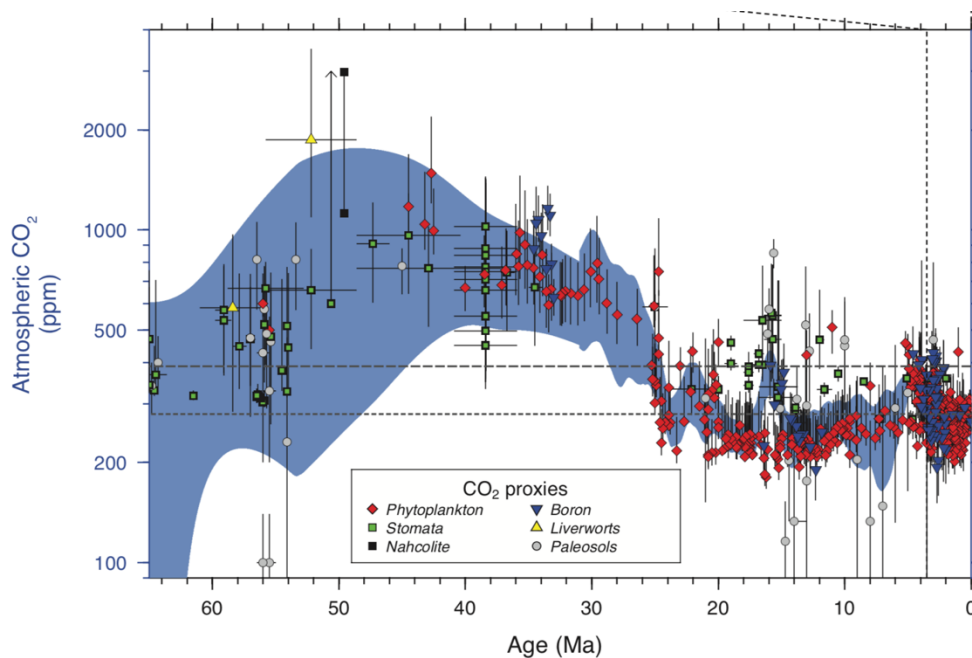


**Figure 4.** Figure 5.2, IPCC 2013. A compilation of reliable paleo-CO<sub>2</sub> proxy reconstructions. Data comes from a variety of papers, and is broken into proxies in the box above. The blue shaded area represents 1 standard deviation calculated with block bootstrap resampling for a kernel regression through all the data points with a bandwidth of 8 Myr prior to 30 Ma, and 1 Myr from 30 Ma to present.

### *The C3 Plant Proxy*

The C3 plant proxy has been proposed in the search for new paleo-CO<sub>2</sub> proxies. This method relies on the fractionation of carbon isotopes during photosynthesis that covaries with  $p\text{CO}_2$ . As  $p\text{CO}_2$  increases, it is expected that the difference in the carbon isotopic composition of leaves relative to the air around them increases (leaf-level carbon isotopic discrimination). In this section, I will describe fractionation in plants, the mechanism for the C3 plant proxy, previous studies that have found this positive relationship, and finally our study.

Plants preferentially incorporate <sup>12</sup>C over <sup>13</sup>C due to a kinetic isotope effect, depicted in Figure 5. This figure shows the energetic profile for a reaction (i.e., reaction coordinate diagram), like carbon fixation, starting with the reactants on the left and progressing to products on the right. In order for a reaction to progress from reactant to transition state (and then to product), the activation energy (difference between reactant energy and transition state energy) must be overcome. The lower the activation energy, the faster a reaction can progress. The zero-point energy (lowest possible energy state) for <sup>13</sup>C is lower than that of <sup>12</sup>C because lighter molecules have more vibrational energy than heavy molecules. This means that the activation energy is greater for <sup>13</sup>C than <sup>12</sup>C. Because <sup>12</sup>C has a smaller activation energy, the rate at which <sup>12</sup>CO<sub>2</sub> goes through the

process of carbon fixation by RuBisCO is faster than that of  $^{13}\text{CO}_2$ . The difference in rates results in the carbon of leaf and plant tissues being depleted in  $^{13}\text{C}$  relative to the composition of atmospheric  $\text{CO}_2$ .

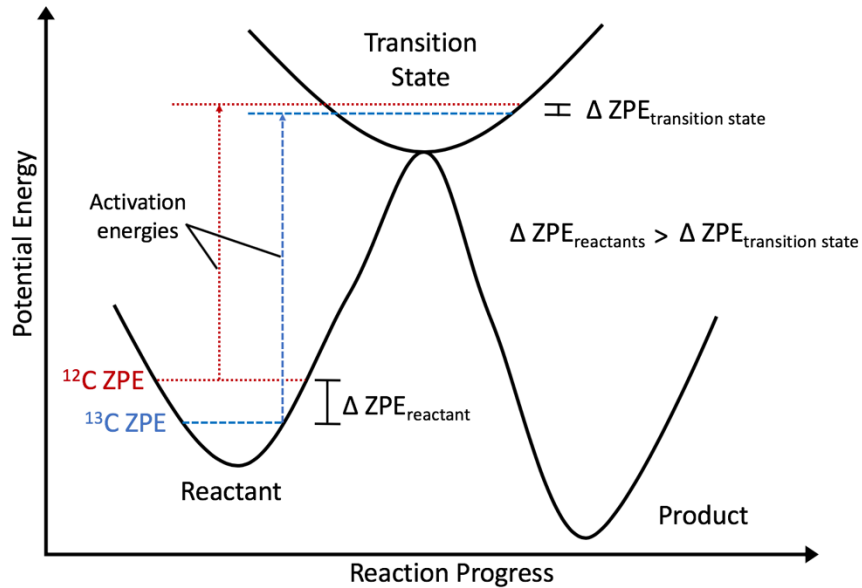


**Figure 5.** A reaction coordinate diagram depicting the kinetic isotope effect. ZPE is zero-point energy.  $\Delta \text{ZPE}_{\text{reactants}}$  represents the difference in ZPE between  $^{13}\text{C}$  and  $^{12}\text{C}$  in the reactant,  $\Delta \text{ZPE}_{\text{transition state}}$  in the product. The  $\Delta \text{ZPE}_{\text{reactants}}$  is larger than the  $\Delta \text{ZPE}_{\text{transition state}}$ . Vertical dashed lines represent activation energies. The blue line ( $^{13}\text{C}$ ) is longer than the red line ( $^{12}\text{C}$ ).

Through the rest of this thesis, there are a few terms that will be repeatedly used in discussion: leaf-level discrimination ( $\Delta^{13}\text{C}$ ), carbon isotopic signature of the leaf ( $\delta^{13}\text{C}_{\text{leaf}}$ ), and carbon isotopic composition of the air ( $\delta^{13}\text{C}_{\text{air}}$ ). These terms are organized in Figure 6 with the equations used to calculate them, as well as a scale bar to familiarize





fractionates against  $^{13}\text{C}$  by  $\sim 27\%$ , PEP carboxylase only fractionates by  $\sim 5.7\%$  [Farquhar et al. 1989]. This makes the carbon isotopic composition of C3 plants much more sensitive to changes in atmospheric  $\text{CO}_2$ , and more useful for a potential paleo- $\text{CO}_2$  proxy.

$$\delta^{13}\text{C} (\text{‰}) = \left( \frac{(^{13}\text{C}/^{12}\text{C})_{\text{sample}}}{(^{13}\text{C}/^{12}\text{C})_{\text{standard}}} - 1 \right) * 1000 \quad (6)$$

$$\Delta^{13}\text{C}_{\text{leaf}} = a + (b - a) \left( \frac{C_i}{C_a} \right) \quad (7)$$

$$\Delta^{13}\text{C}_{\text{leaf}} = \frac{\delta^{13}\text{C}_{\text{air}} - \delta^{13}\text{C}_{\text{leaf}}}{1 - \left( \frac{\delta^{13}\text{C}_{\text{leaf}}}{1000} \right)} \quad (8)$$

Equation 7 shows the relationship between fractionation during diffusion into the stomata (“a”), fractionation during carbon fixation (“b”), the ratio of internal  $p\text{CO}_2$  to external  $p\text{CO}_2$  ( $C_i/C_a$ ), and  $\Delta^{13}\text{C}_{\text{leaf}}$ .  $\Delta^{13}\text{C}_{\text{leaf}}$  (or carbon isotope discrimination) is measured for plants: the carbon isotopic composition ( $\delta^{13}\text{C}$ , Equation 6) of the leaf and the atmosphere that the leaf grew in are measured, and Equation 8 is used to calculate  $\Delta^{13}\text{C}_{\text{leaf}}$ . The relative impact of the fractionations represented by “a” and “b” in Equation 7 is dependent upon the  $C_i/C_a$  ratio. With low  $C_i/C_a$ ,  $\Delta^{13}\text{C}_{\text{leaf}}$  approaches “a”, the fractionation from  $\text{CO}_2$  diffusing through the stomata, which is only 4.4 ‰. With high  $C_i/C_a$ ,  $\Delta^{13}\text{C}_{\text{leaf}}$  approaches “b”. In C3 plants, the value for “b” is  $\sim 27\%$  from RuBisCO fractionation, so there is a lot of change in  $\Delta^{13}\text{C}_{\text{leaf}}$  with change in  $C_i/C_a$ . In C4 plants, however, the value for “b” is a combination of PEP carboxylase fractionation ( $\sim 5.7\%$ )

and other steps which can vary, giving “b” a variable and smaller value than for RuBisCO in C3 plants [Farquhar et al. 1989]. Therefore, changes in  $C_i/C_a$  would result in much more variable and smaller changes in  $\Delta^{13}C_{\text{leaf}}$  than in C3 plants. It is for this reason that the proxy method investigated in this work utilizes C3 plants for  $\Delta^{13}C_{\text{leaf}}$  measurements instead of C4 plants.

Carbon isotope discrimination changes with the  $C_i/C_a$  ratio, following Equation 7. The C3 plant proxy method relies on increasing  $C_i/C_a$  with  $pCO_2$ . As atmospheric  $pCO_2$  increases,  $C_i$  also increases relative to  $C_a$ , so long as plants do not respond to changing  $pCO_2$  by closing their stomata. Increasing  $C_i$  causes an increased expression of fractionation due to RuBisCO, bringing the  $\Delta^{13}C_{\text{leaf}}$  value closer to “b” (larger). With increasing  $pCO_2$ , in theory we would expect to see an increase in the leaf-level carbon isotope discrimination ( $\Delta^{13}C_{\text{leaf}}$ ) in a plant (Figure 7).

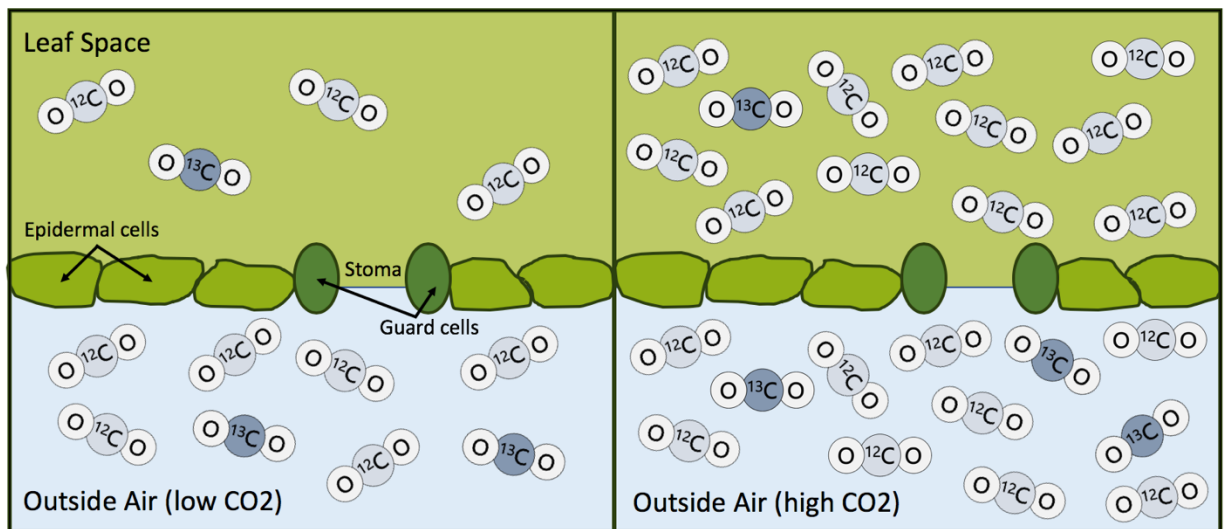


**Figure 7.** A cartoon of carbon isotope discrimination. On the left pane, in a low  $CO_2$  scenario, the internal leaf space (green) has half the  $CO_2$  of the air (blue), giving a  $C_i/C_a$  of 0.5. Both the internal  $CO_2$  and the  $CO_2$  of the air have the same carbon isotopic composition (dark blue C is  $^{13}C$ , light blue is  $^{12}C$ ). On the right pane, in a high- $CO_2$

scenario, the  $C_i/C_a$  is higher at 1, and the composition of  $\text{CO}_2$  in the leaf is more depleted in  $^{13}\text{C}$  than the surrounding air, as RuBisCO preferentially incorporates  $^{12}\text{C}$ .

In order to determine the validity of this theory, studies have been carried out where C3 plants are grown under different atmospheric  $\text{CO}_2$  concentrations. The idea is that if this relationship is present in C3 plant species, a calibration curve of  $\Delta^{13}\text{C}_{\text{leaf}}$  versus  $p\text{CO}_2$  can be generated. Then, fossil plants can be analyzed for their carbon isotopic composition ( $\delta^{13}\text{C}_{\text{leaf}}$ ) and used with known  $\delta^{13}\text{C}_{\text{air}}$  to calculate  $\Delta^{13}\text{C}_{\text{leaf}}$ . With  $\Delta^{13}\text{C}_{\text{leaf}}$ ,  $p\text{CO}_2$  can be calculated from the calibration curve. Schubert and Jahren observed the expected positive correlation between  $\Delta^{13}\text{C}_{\text{leaf}}$  and  $p\text{CO}_2$  [2012]. In this study, two C3 species, *Arabidopsis thaliana* (rockcress) and *Raphanus sativus* (radish) were grown in growth chambers under 7 and 8 levels of  $p\text{CO}_2$ , respectively, ranging from 370-2255 ppm and 407-4200 ppm, respectively. In bulk *n*-alkanes (extracted from leaves), above-ground and below-ground tissue for *R. sativus* bulk and above-ground tissue for *A. thaliana*, a positive hyperbolic relationship was found between  $\Delta^{13}\text{C}_{\text{leaf}}$  and  $p\text{CO}_2$  (Figure 8).

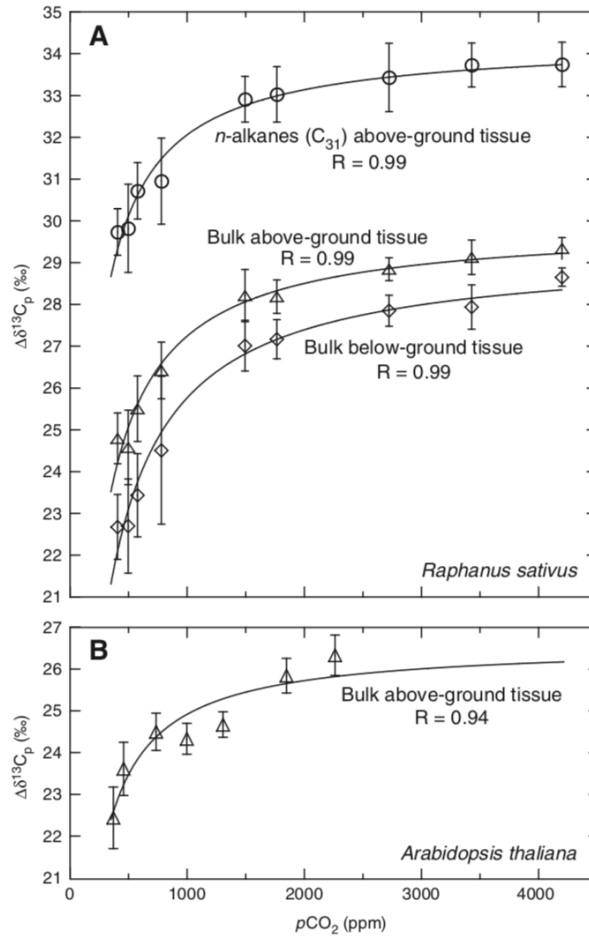


**Figure 8.** Figure 2 Schubert and Jahren 2012.  $\Delta^{13}C_{leaf}$  versus  $pCO_2$  for *R. sativus* tissues and *A. thaliana* tissues. Error bars represent one standard deviation. A hyperbolic curve was fit to the data.

Unfortunately, small annual plants like *R. sativus* and *A. thaliana* are not well preserved in the fossil record, so these calibration curves cannot be directly applied to fossils of the same lineage. In order to use this observed positive relationship between  $\Delta^{13}C_{leaf}$  and  $pCO_2$ , similar studies must be carried out with plants that are relevant to the fossil record: the same species is present in the fossil record, or there are very similar species present in the fossil record.

*Ginkgo* is a popular taxon for paleoclimate reconstructions given its extremely long fossil record and excellent preservation. The genus *Ginkgo* goes back to the Jurassic [Tralau 1968], and has changed very little morphologically over the past 100 million years [Zhou and Zhang 2003]. *Ginkgo* is also extremely well preserved in the fossil record, with intact leaf cuticle often being found. At the time of the PETM, *Ginkgo wyomingensis* was extant. Today, *Ginkgo biloba* is the only living species, and looks nearly identical to extinct *G. wyomingensis*. This unique preservation allows for the possibility to do many kinds of studies: morphological, anatomical, and chemical. The ability to reconstruct paleo-CO<sub>2</sub> from *Ginkgo* is of particular interest because of the large amounts of *Ginkgo wyomingensis* cuticle that have been collected surrounding the PETM in the Bighorn Basin, Wyoming.

*Ginkgo* has been used for paleo-CO<sub>2</sub> proxies (stomatal index). These studies have used herbarium sheets (going back to pre-industrialization), modern samples, and experimental leaves grown under elevated CO<sub>2</sub> [Barclay and Wing 2016]. There are limited data to correlate *Ginkgo* under high CO<sub>2</sub> conditions (~400-1000 ppm). To be applicable to periods like the PETM, extant *G. biloba* must be thoroughly studied under elevated CO<sub>2</sub> levels.

In 2016, 15 mature *Ginkgo* trees (~1.5m) were planted in an experimental plot, and surrounded by open-topped chambers. CO<sub>2</sub> was pumped into these chambers to reach *p*CO<sub>2</sub> levels ranging from ambient (~410 ppm) -1000 ppm. Growing mature trees in an outdoor setting over several years has a few advantages. Many types of studies can be conducted on these plants: samples can be taken to look at stomatal index and carbon isotopic composition, physiological measurements can be made on these plants, and

environmental conditions captured. With all of this data coming from one experimental plot, it is possible to investigate questions of plant physiology in elevated CO<sub>2</sub> conditions, as well as several paleo-CO<sub>2</sub> proxies, namely the stomatal index proxy [Barclay and Wing 2016], carbon isotope discrimination (C3 plant proxy), and the Franks method which uses isotopic measurements in conjunction with anatomical measurements to estimate  $p\text{CO}_2$  [Franks et al. 2014]. These trees are growing under real environmental conditions, so while they are watered to avoid stress, they do experience real seasonality, weather patterns, etc. These are the same environmental variables that would also have been recorded in the leaves of trees that were preserved in the fossil record. Our experiment is therefore different than well-controlled growth chamber experiments in being more analogous to the plants preserved in the fossil record and the conditions that they grew under. The subject of this study is the carbon isotopic discrimination of these *G. biloba* trees under elevated CO<sub>2</sub>.

### ***Materials and Methods***

**Summary:** In order to assess the effect of elevated  $p\text{CO}_2$  on leaf-level carbon isotope discrimination ( $\Delta^{13}\text{C}_{\text{leaf}}$ ) in *Ginkgo biloba*, *G. biloba* trees were grown under elevated  $p\text{CO}_2$  conditions. Leaves from these trees and the air from around the canopy were sampled and analyzed for  $\delta^{13}\text{C}$  using an elemental analyzer isotope ratio mass spectrometer (EA/IRMS). Average air  $\delta^{13}\text{C}$  values were calculated from the sampled  $\delta^{13}\text{C}_{\text{air}}$  values with a mixing line and the measured average  $[\text{CO}_2]$  for each tree.  $\Delta^{13}\text{C}_{\text{leaf}}$  was calculated from the calculated  $\delta^{13}\text{C}_{\text{air}}$  and the measured  $\delta^{13}\text{C}_{\text{leaf}}$  values, following Equation 7.

**Trees grown Under Elevated  $\text{CO}_2$ :** *Ginkgo biloba* trees have been growing since 2016 under experimental conditions outdoors in a field surrounded by mature trees at the Smithsonian Environmental Research Center in Edgewater, MD. All *G. biloba* trees are male and of the variety Presidential Gold grafted onto root stock to reduce genetic variability. Each tree is in an open-topped chamber, under ambient light and temperature fluctuations and exposed to natural precipitation (Figure 9A). There are three trees at each  $\text{CO}_2$  level: 1000, 800, 600, and  $\sim 400$  ppm (ambient, no  $\text{CO}_2$  added), and an additional 3 trees outside of chambers under ambient conditions. Treatment levels are randomized following a randomized block design, with three rows that each contain all treatment levels (Figure 9B). In early Spring of 2019, saplings in small pots were added to each chamber.  $\text{CO}_2$  is added to chambers at the intake of the blower fans, and levels are monitored and recorded in each chamber (or next to outdoor trees) with a LiCOR 7000 gas analyzer.  $\text{CO}_2$  levels are adjusted as needed via flowmeters in the control shed.



The air inside each chamber is replaced every few minutes by new air blowing in, so people breathing while moving in and out of the chambers to take measurements, perform maintenance, etc. does not have a significant effect on CO<sub>2</sub> levels. Shade cloth was added to the experiment in the summer of 2018. Trees are watered as necessary, and occasionally fertilized. Eight environmental parameters are measured within the chambers every minute: CO<sub>2</sub> concentration, relative humidity, air temperature, soil moisture, soil temperature, photosynthetically active radiation (PAR), a measure of plant-reflected light (NDVI), and the photochemical reflected index (PRI).



**Figure 9.** Experimental setup at the Smithsonian Environmental Research Center in Edgewater, Maryland. Trees are in open-topped chambers aside from outdoor control trees (pictured on the left). The control shed houses monitoring equipment as well as the supply of CO<sub>2</sub>. Blowers combine ambient air and CO<sub>2</sub> from the control shed into each of the chambers.

**Green Leaf Sampling:** In the Summer of 2018, leaves were sampled for 11 weeks through the growing season, from 4/18 through 6/20. The first week of sampling occurred when leaves were barely large enough to be sampled (sometimes less than 1 cm). In trees with large canopies, the  $\delta^{13}\text{C}_{\text{leaf}}$  value can vary through the canopy depending on how

central the leaf is or the distance of the leaf to the ground. Our trees have relatively small canopies, but it was still necessary to test for variability in  $\delta^{13}\text{C}_{\text{leaf}}$  within each tree. Three to six leaves were taken from the bottom of the North side (low and more shaded) and top of the South side (high and in the full sun) of each mature tree, sampling along the same branch on both sides for the season. After determining that there was no significant difference between leaves taken from the North or South side of each tree, leaves in 2019 were sampled only on the South side, on the same branch and locations as 2018, from 4/17 through 6/19. Leaves were also sampled from saplings every other week over the same period, less than the large trees to limit the destruction of their canopy. These saplings in pots were added to the experiment before the beginning of the growing season in 2019. They are the same variety (Presidential Gold) as the large trees and are also grafted to root stock, but are only about 50 cm tall.

***Abscised Leaf Sampling:*** Abscised leaves from Fall 2015 were collected from the ground around trees before they had entered experimental conditions. Leaves from the Fall of 2016 through the Fall of 2018 were collected from the ground within each chamber.

***Leaf preparation:*** Leaves collected from the ground in the Fall of 2015 were first brushed to remove dirt, then soaked in 5% HCl for 48 hours to remove any inorganic carbon from the surface (e.g., carbonate minerals). Excess HCl was poured off, and leaves were rinsed 4x with DI water before being air dried. For all leaves, an image was taken, the leaf dried for 48 hours at 40°C in an oven, and the mass of the leaf recorded. The petiole (stem) of the leaf and half of the blade was saved, and the other half of the

blade used for analysis (Figure 10). The half-blades were then ground to a powder in a ceramic mortar and pestle that was washed between leaf samples with acetone. When leaves were too small, more than half of the blade was ground. For very early leaves (from the first week of sampling), the entire leaf including the petiole was ground. Leaf powders were transferred to small, labeled glass vials.

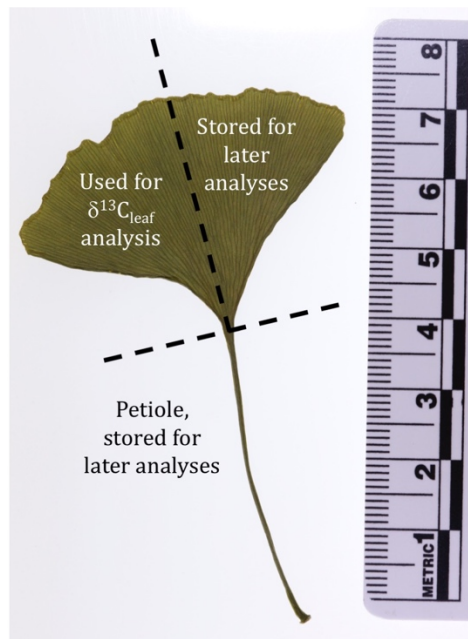


**Figure 10.** *Ginkgo biloba* leaf from week 6 of the 2019 growing season. Dashed lines show where this leaf was cut with a razor blade, removing the petiole and halving the blade of the leaf.

**Elemental Analyzer-Isotope Ratio Mass Spectrometry (EA-IRMS):** EA-IRMS was used to analyze the carbon isotopic composition of leaf samples ( $\delta^{13}\text{C}_{\text{leaf}}$ ) (Figure 11). About 5 mg of homogenized powder from each was weighed into a small tin boat. The tin boat was then flattened and folded into a tin cube containing the sample. The sample-containing tin cube was dropped into the furnace of the Elemental Analyzer. Here, the

sample immediately combusts in the presence of  $O_2$  to evolve  $CO_2$ ,  $H_2O$ ,  $SO_2$ ,  $N_2$ ,  $NO_2$ , and  $NO$ . This mixture of gases then enters a reduction column where excess  $O_2$  and nitrogen oxides are scrubbed out of the gas mixture, forming  $CuO$  and producing elemental nitrogen gas from the nitrous oxides. The gases move through a water trap where  $H_2O$  gas is removed by a drying agent (such as magnesium perchlorate) before the gas chromatography column where the remaining gas species are separated. Then, the eluent flows through a thermal conductivity detector (TCD) where each gas species is quantified on its way to the IRMS. First, two pulses of a nitrogen reference gas are flowed through the system, followed by the sample  $N_2$  gas, then the sample  $CO_2$  gas followed by two pulses of a  $CO_2$  reference gas. The gas is ionized, and a magnetic field is applied to separate masses 28 and 29 for  $N_2$ , and 44, 45, and 46 for  $CO_2$ . Between  $N_2$  samples and  $CO_2$  samples, the magnetic field is adjusted to properly separate the masses and align each mass with one of three Faraday cups, which measure the abundance of each mass from the current produced by ions hitting the cup. From the EA-IRMS setup, weight percent and isotopic data is collected for both N and C.

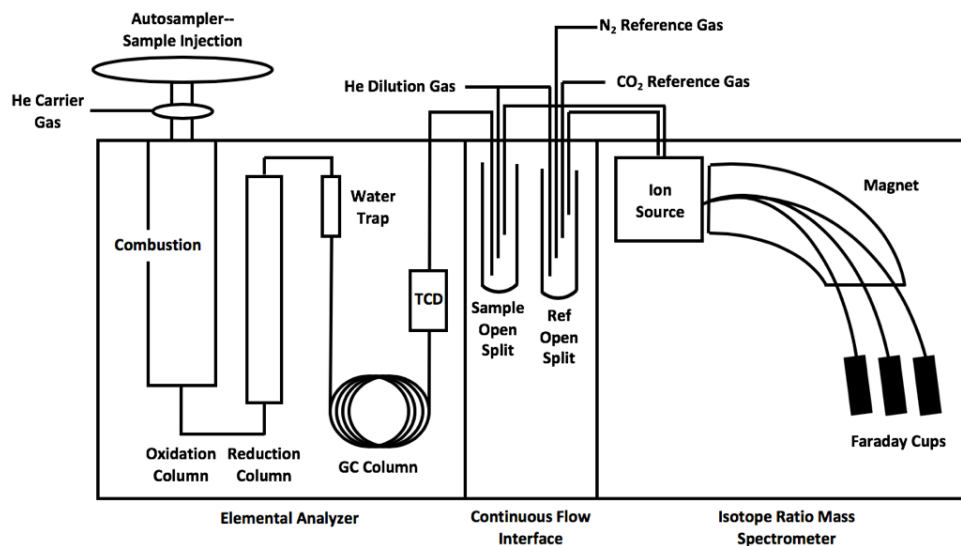


**Figure 11.** Cartoon of EA-IRMS. The sample enters the EA where it combusts, and the evolved gases move through the reduction column, water trap, gas chromatography column, thermal conductivity detector (TCD), then to the continuous flow interface. From there, the sample becomes ionized in the ion source before the masses are separated by the magnet and each mass is collected in one of three Faraday cups.

The raw data output from the IRMS system is the current from each of the three Faraday cups with a retention time (Figure 12). The software associated with the instrument (Thermo ISODAT) defines peaks and integrates under the peak to give an area that corresponds to the abundance of that  $m/z$  value in the sample. The software corrects for the contribution of isotopologues containing  $^{17}\text{O}$  (Table 1). Once corrected, the instrument then uses the ratio of masses to produce a  $\delta^{13}\text{C}$  value.

$m/z$ value	Isotopologues
44	$^{12}\text{C}^{16}\text{O}^{16}\text{O}^+$
45	$^{13}\text{C}^{16}\text{O}^{16}\text{O}^+$ , $^{12}\text{C}^{17}\text{O}^{16}\text{O}^+$
46	$^{12}\text{C}^{16}\text{O}^{18}\text{O}^+$ , $^{13}\text{C}^{17}\text{O}^{16}\text{O}^+$ , $^{12}\text{C}^{17}\text{O}^{17}\text{O}^+$

**Table 1.** Isotopologues are listed for each  $m/z$  value measured in the analysis of  $\text{CO}_2$ . For  $m/z$  45 and 46, the  $^{17}\text{O}$  correction must be made to the data to avoid miscalculating the ratio of  $^{13}\text{C}$  to  $^{12}\text{C}$ .

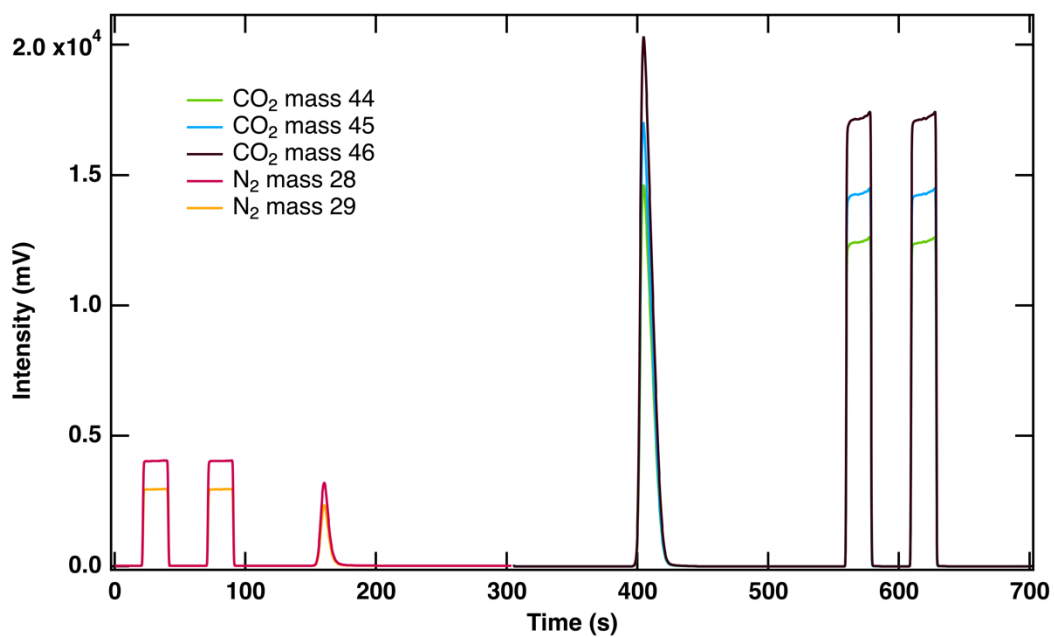


**Figure 12.** Output from EA/IRMS setup. Two peak of reference  $\text{N}_2$  are analyzed before the sample  $\text{N}_2$  peak. Then, the sample  $\text{CO}_2$  peak is analyzed, followed by two samples of reference  $\text{CO}_2$ .

After calculating the  $\delta$  values from the raw instrument output, these values still have to be corrected using standards, both reference and in-house. In this work, the most common combination of standards for a run was Peru Mud (in house), L-glutamic Acid (reference) and Urea 1 (reference), with certified carbon isotopic compositions of  $-20.29\text{‰}$ ,  $-26.389\text{‰}$ , and  $-31.43\text{‰}$ , respectively. The measured values for the standards are plotted against these certified values, and are fit to a line (Figure 13). The equation of this line is then used to normalize the  $\delta$  values of the leaf samples, and these values become the real, reported data.

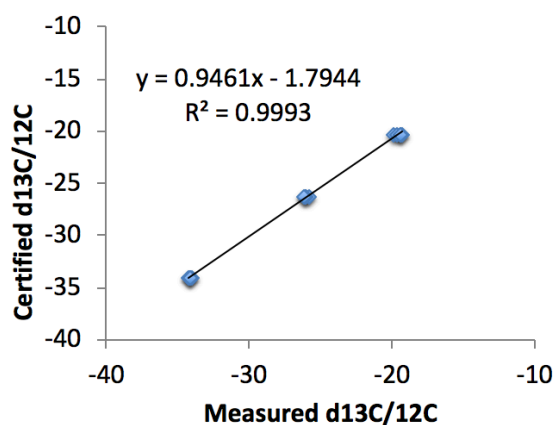


**Figure 13.** Certified  $\delta^{13}\text{C}$  values of standards plotted against measured  $\delta^{13}\text{C}$  during an EA/IRMS run. The equation of the line of best fit is  $y=0.9461x-1.7944$ ,  $R^2=0.9993$ .

In this study, carbon and nitrogen isotope ratios and weight percent TOC and TON were measured in duplicate using a FlashEA 1112 Isolink that was coupled via a ConFlo IV universal interface to the DELTA V Plus isotope ratio mass spectrometer (Thermo Fisher Scientific) with a universal triple collector. The Flash EA consisted of a zero blank autosampler, a single combustion-reduction reactor (18 mm o.d., 14 mm i.d., 45.4 cm long) filled with  $\text{WO}_3$  and reduced copper grains and operated at  $1020^\circ\text{C}$ , a water trap (glass tube, 11 cm long, 8 mm i.d., plastic end-fittings with Teflon/rubber O-rings) containing magnesium perchlorate, a packed GC column for separation of analyte gases (sulfinert separation column PP-QS, 2 m, 1/4", 50/80 mesh, Restek PC4974), and a thermal conductivity detector (TCD). A magnetic field jump of the IRMS was automatically programmed between the  $\text{N}_2$  and  $\text{CO}_2$  peaks and the  $\text{CO}_2$  and  $\text{SO}_2$  peaks. Carbon and nitrogen isotope values are reported in delta notation normalized to the internationally recognized standards Vienna Pee Dee belemnite (VPDB) and AIR,

respectively, using reference standards Urea 1 (Indiana University) and L-glutamic acid (USGS 40) and two in-house standards: Peru Mud and Cornstarch.

The in-house standards are measured against internationally recognized standards (for carbon, Vienne Pee Dee Belemnite or VPDB) to come to a certified  $\delta^{13}\text{C}$  value for the in-house standards (Equation 9). These standards are then used to calibrate the measurements made during a run.

$$\delta^{13}\text{C} (\text{‰}) = \left( \frac{(^{13}\text{C}/^{12}\text{C})_{\text{in-house standard}}}{(^{13}\text{C}/^{12}\text{C})_{\text{VPDB}}} - 1 \right) * 1000 \quad (9)$$

**Air Sampling:** Air sampling was carried out to determine the  $\delta^{13}\text{C}_{\text{air}}$  value needed to calculate  $\Delta^{13}\text{C}_{\text{leaf}}$  with  $\delta^{13}\text{C}_{\text{leaf}}$  (Equation 8). Air samples were collected in flasks the same day as leaf sampling in the summers of 2018 and 2019, with some extra samples taken through the week prior to sampling in 2019. Air was sampled next to each tree, inside experimental chambers, and from the  $\text{CO}_2$  source dewar weekly. An air pump was connected via hosing to a collection flask under vacuum. The pump moved air through the opened flask for a period of two minutes before being closed off. Air samples were analyzed for stable carbon isotopes and  $\text{pCO}_2$  at the SIRFER Lab in Utah via dual-inlet IRMS, which is very similar to the system used for leaf isotope analysis. Instead of combusting the sample in a tin boat, the sample gas is introduced directly to the instrument, alternating with a reference gas.



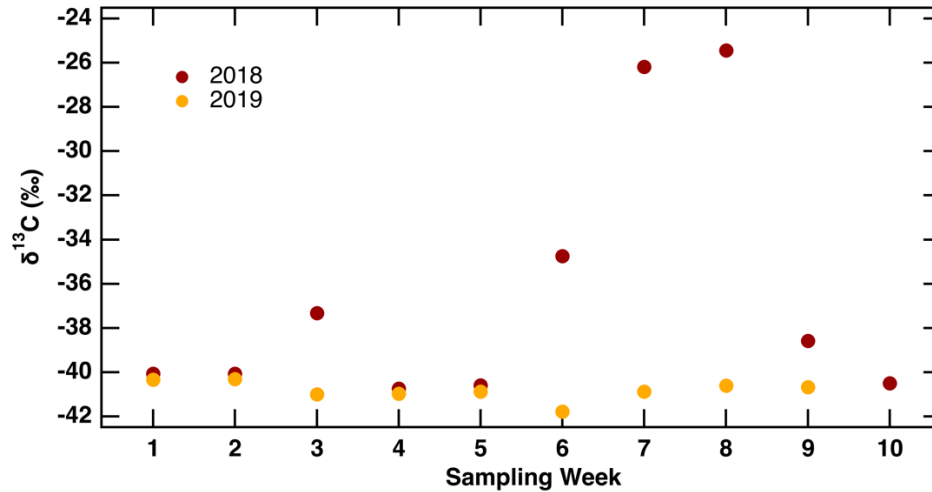


**Figure 14.**  $\delta^{13}\text{C}$  values from the source of added  $\text{CO}_2$  through each week of leaf sampling in both 2018 (red circles) and 2019 (orange circles).  $\delta^{13}\text{C}$  values from 2019 show far less variability than from 2018.

In our calculation of  $\delta^{13}\text{C}_{\text{air}}$ , we need to account for 2 variables: (1) the changing  $\delta^{13}\text{C}$  value of added air from the dewars from week to week (Figure 14) and (2) the different ratio of ambient  $\text{CO}_2$  to added  $\text{CO}_2$  in each chamber, we took weekly air samples from each chamber. Ambient air has a  $\delta^{13}\text{C}_{\text{air}}$  value of  $\sim -10\text{‰}$ . If the  $\text{CO}_2$  that we added to the elevated  $\text{CO}_2$  chambers also had a consistent  $\delta^{13}\text{C}_{\text{air}}$  value of  $\sim -10\text{‰}$ , we would not need to take air samples and could use  $-10\text{‰}$  as the  $\delta^{13}\text{C}_{\text{air}}$  value in all calculations for  $\Delta^{13}\text{C}_{\text{leaf}}$  (Equation 8). Unfortunately, the  $\text{CO}_2$  that is added to chambers to raise the  $[\text{CO}_2]$  to 600, 800, and 1000 ppm has a variable composition that is much more depleted in  $^{13}\text{C}$  than ambient air. The dewars depicted in Figure 8 on the control shed are replenished weekly with  $\text{CO}_2$  from industrial sources. Through the 2018 growing season, the  $\delta^{13}\text{C}$  of the added  $\text{CO}_2$  was quite variable, ranging from  $-40.75$  to  $-25.45\text{‰}$  (Figure 14). In 2019, it was far more consistent, the average  $-40.83\text{‰}$  with a very small standard deviation of  $0.44\text{‰}$ . In elevated  $\text{CO}_2$  chambers, ambient air ( $-10\text{‰}$ ) is mixed with the  $^{13}\text{C}$

depleted dewar air (-40.75 to -25.45‰) to give an intermediate value that decreases in  $\delta^{13}\text{C}$  with increasing chamber  $[\text{CO}_2]$  as more of the  $^{13}\text{C}$ -depleted  $\text{CO}_2$  is added.

When the air samples are analyzed, a value for  $\delta^{13}\text{C}_{\text{air}}$  is received along with the  $[\text{CO}_2]$  of the sample. A mixing line (Fig. 15) was constructed for each week using the data from air samples.  $\delta^{13}\text{C}$  of each sample was plotted against the proportion of added  $\text{CO}_2$ , calculated with Equation 10: Using the ambient  $[\text{CO}_2]$  value from the air flask samples, the proportion of added  $\text{CO}_2$  average for the week is calculated. The  $\delta^{13}\text{C}_{\text{air}}$  value for every chamber falls along this line for the week: the higher the  $[\text{CO}_2]$  and the proportion of dewar air, the more negative the  $\delta^{13}\text{C}_{\text{air}}$  value, and the more  $^{13}\text{C}$ -depleted that air is. The points that create this line represent each air sample that was taken that week.

The  $[\text{CO}_2]$  from gas samples is just a snapshot in time: these samples establish the mixing line for the week, but do not accurately represent the  $[\text{CO}_2]$  in each chamber. The average daytime  $[\text{CO}_2]$  for each chamber for each week was calculated with the LiCOR gas analyzer data taken every 15 minutes. Using the ambient  $[\text{CO}_2]$  value from the air flask samples for the week, the proportion of added  $\text{CO}_2$  for the week is calculated. The equation of the mixing line is then used to calculate average weekly  $\delta^{13}\text{C}_{\text{air}}$  from the proportion of added  $\text{CO}_2$ :

$$\textit{Proportion of added } \text{CO}_2 = \frac{[\text{CO}_2]_{\text{sample}} - [\text{CO}_2]_{\text{ambient}}}{[\text{CO}_2]_{\text{sample}}} \quad (10)$$

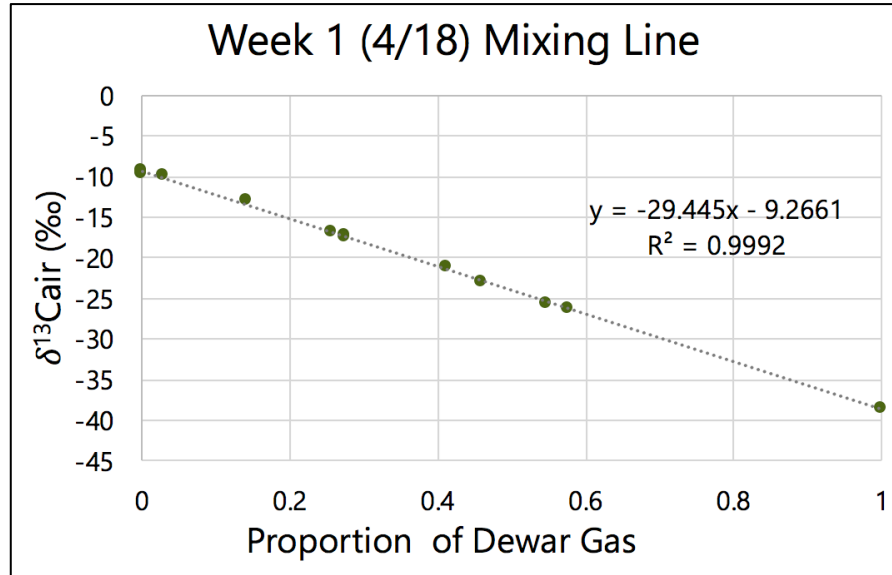


**Figure 15.** Sample mixing line of ambient air and dewar CO<sub>2</sub>. Plotting the isotopic composition of the air against the proportion of dewar gas added to the chamber gives a linear relationship used to calculate average δ<sup>13</sup>C values of the atmosphere for each week of the experiment.

Below is a table of values used to calculate δ<sup>13</sup>C<sub>air</sub> for each week of sampling in 2018 and 2019:

Leaf Collection Year Week	Ambient pCO <sub>2</sub> (ppm)	Ambient δ <sup>13</sup> C (‰)	Dewar δ <sup>13</sup> C (‰)	Mixing line equation	R <sup>2</sup>
2018	1	420.81	-9.34	$y = -30.81x - 9.63$	0.9984
	2	420.81	-9.34	$y = -30.81x - 9.63$	0.9984
	3	427.41	-10.11	$y = -27.60x - 10.28$	0.9973
	4	430.26	-9.81	$y = -30.95x - 10.20$	0.9981
	5	425.52	-10.19	$y = -30.94x - 10.01$	0.9945
	6	425.86	-9.50	$y = -25.78x - 9.67$	0.9989
	7	427.70	-10.12	$y = -16.44x - 10.31$	0.9948

















	8	453.56	-11.09	-25.451	$y = -14.57x - 10.98$	0.9940	
	9	411.45	-9.42	-38.578	$y = -29.35x - 9.32$	0.9987	
	10	401.74	-8.92	-40.501	$y = -31.50x - 9.09$	0.9987	
	11	442.91	-10.12	-	$y = -23.78x - 10.13$	0.9844	
	2019	1	419.67	-9.56	-40.333	$y = -31.04x - 9.28$	0.9955
		2	423.80	-9.57	-40.308	$y = -30.69x - 9.62$	0.9995
		3	419.41	-9.26	-40.996	$y = -32.19x - 9.27$	0.9984
		4	424.63	-9.15	-40.973	$y = -31.84x - 9.14$	0.9999
		5	422.22	-	-40.874	$y = -32.04x - 8.87$	0.9992
		6	422.22	-	-41.786	$y = -32.95x - 8.84$	0.9994
7		419.81	-9.03	-40.873	$y = -31.84x - 9.03$	0.9995	
8		449.33	-8.84	-40.61	$y = -32.08x - 8.53$	0.9986	
9		396.88	-7.95	-40.683	$y = -32.63x - 8.06$	1.0000	
10		472.85	-11.86	-	$y = -28.96x - 11.86$	1.0000*	

**Table 2.** Air data for leaf sampling weeks from both 2018 and 2019. Cells marked with “-” represent missing data (broken flask, bad data acquisition). In the mixing line equation, y is  $\delta^{13}\text{C}_{\text{air}}$  and x is the proportion of the added  $\text{CO}_2$  in the sample. \*- only contains two data points

**$\Delta^{13}\text{C}_{\text{leaf}}$  calculations:** The  $\delta^{13}\text{C}_{\text{leaf}}$  and  $\delta^{13}\text{C}_{\text{air}}$  were used in Equation 8 from Farquhar et al. 1989 was used for the calculation of  $\Delta^{13}\text{C}_{\text{leaf}}$ . Leaf values were paired with air values from the weeks prior to collecting the leaf. A leaf collected on 6/5/19 was composed of carbon from  $\text{CO}_2$  that had been incorporated before that collection day. Therefore, if the leaf was collected in week 8, then the air values from weeks 1-7 were averaged for the

$\delta^{13}C_{air}$  value used in Equation 7 (Figure 15). In the case of 2015, 2016, and 2017 abscised leaves for which no air data was collected, average air composition values from the summer of 2018 were used for  $\Delta^{13}C_{leaf}$  calculations.

$$\Delta^{13}C_{leaf} = \frac{\delta^{13}C_{air} - \delta^{13}C_{leaf}}{1 - (\delta^{13}C_{leaf}/1000)} \quad (8)$$

Date	4/17/19	4/24/19	5/1/19	5/8/19	5/15/19	5/22/19	5/29/19	6/5/19	6/12/19	6/19/19
Sampling Week	1	2	3	4	5	6	7	8	9	10
$\delta^{13}C_{air}$ Sampling	Yes	Yes	Yes	Yes	Yes	Yes	Yes	Yes	Yes	Yes
$\delta^{13}C_{leaf}$ Sampling (Large Trees)										
$\delta^{13}C_{leaf}$ Sampling (Small Trees)			NA		NA		NA		NA	

**Figure 16.** Sampling timeline for 2019. Air samples were collected once a week for ten weeks, large trees had leaves collected once a week, and small trees were collected for the first two weeks and every other week for the ten-week period. Images are from trees in 800 ppm CO<sub>2</sub> chambers. All leaf images are normalized to the same scale. The  $\delta^{13}C_{leaf}$  values for the leaves outlined in orange would be paired with the average of weeks of  $\delta^{13}C_{air}$  samples outlined in orange.

## Results

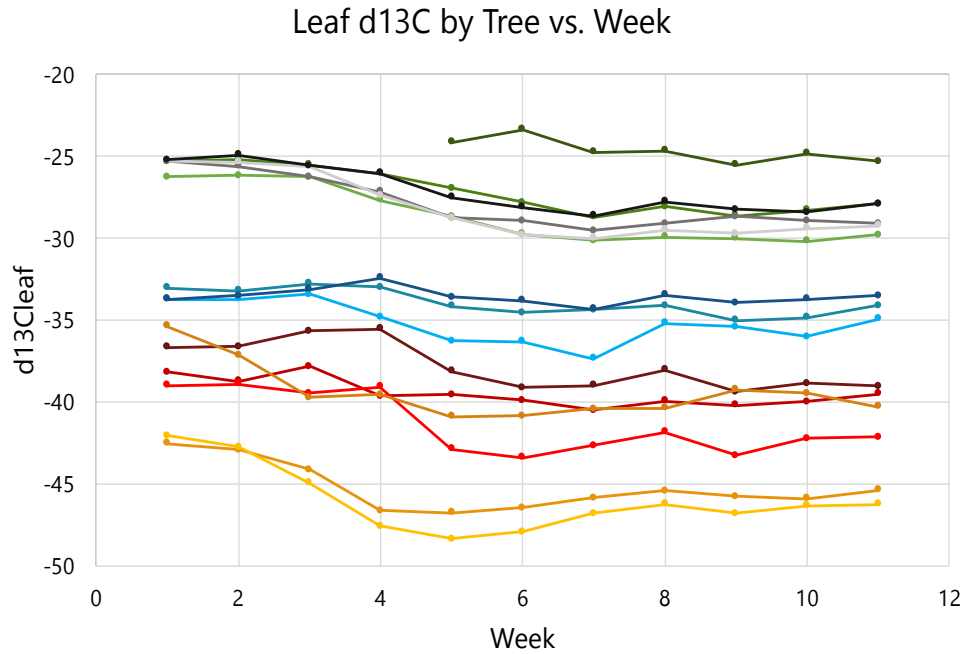


**Figure 17.**  $\delta^{13}\text{C}_{\text{leaf}}$  values for each tree through the 2018 growing season. A similar pattern is seen in the 2019 data, not plotted. Grey lines represent outdoor ambient trees, green lines in-chamber ambient trees, blue lines 600 ppm trees, red lines 800 ppm trees, and orange lines 1000 ppm trees.

Over the course of the 2018 growing season, we saw a decline in the  $\delta^{13}\text{C}_{\text{leaf}}$  values from every tree with an average decline of  $2.86 \pm 1.38\%$  over the 11-week sampling period (Figure 17). This seasonal decline is due to changing leaf diffusivity. When leaves first develop, they lack airspaces and mature stomata which are necessary for photosynthesis. With development, airspaces and stomata increase in size, thereby increasing diffusivity, and the internal  $\text{CO}_2$  concentration of the leaf ( $C_i$ ).  $C_i$  is the main driver for  $\Delta^{13}\text{C}_{\text{leaf}}$ , and from Equation 7, as  $C_i$  increases relative to  $C_a$ , so does  $\Delta^{13}\text{C}_{\text{leaf}}$ , so increasing  $C_i$  through the growing season produced a decline in  $\delta^{13}\text{C}_{\text{leaf}}$ . The same process occurs no matter what treatment level of  $\text{CO}_2$  the tree is subjected to—diffusivity will change over the course of the growing season regardless.

A decline of the same magnitude was observed in the 2019 growing season as well. Because the leaf values level off at week 6-7 (Figure 17), we decided to use only the last four weeks (weeks 8-11 from 2018 and 7-10 in 2019) in our calculations of  $\Delta^{13}\text{C}_{\text{leaf}}$ . This way, we were able to compare values between treatments without having to consider that offsets could be due to differences in the timing of airspace development between trees.

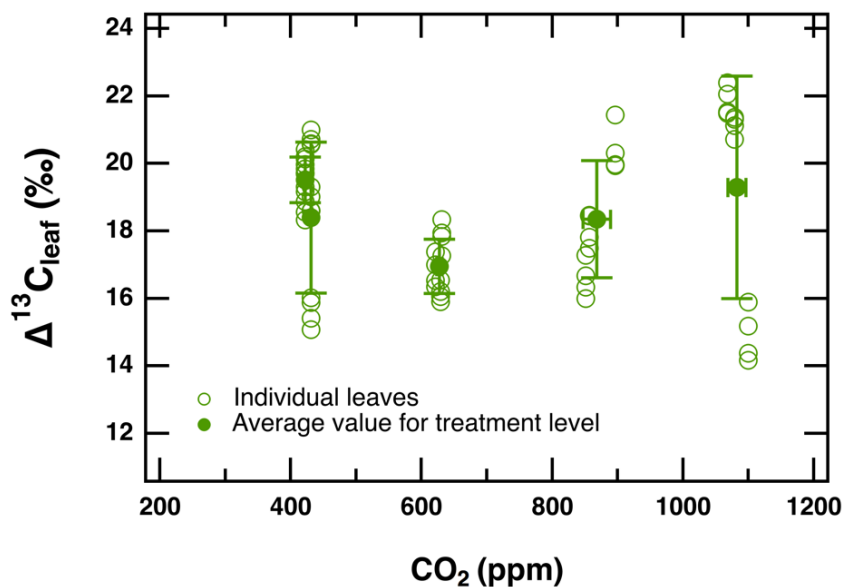


**Figure 18.**  $\Delta^{13}\text{C}_{\text{leaf}}$  values from the last four weeks of the 2018 growing season. Open circles represent individual leaves. Filled circles represent the average  $\Delta^{13}\text{C}_{\text{leaf}}$  value for each treatment level. Horizontal error bars represent one standard deviation in the actual  $[\text{CO}_2]$  of each chamber, and vertical one standard deviation of  $\Delta^{13}\text{C}_{\text{leaf}}$  values.

In 2018, we found an unexpected relationship between  $\Delta^{13}\text{C}_{\text{leaf}}$  and  $p\text{CO}_2$  (Figure 18). The expectation is that as  $p\text{CO}_2$  increases,  $C_i$  also increases, yielding a higher  $\Delta^{13}\text{C}_{\text{leaf}}$  value. Rather than increasing  $\Delta^{13}\text{C}$  with increasing  $p\text{CO}_2$ , in 2018 we saw a decrease in  $\Delta^{13}\text{C}$  from ambient trees ( $19.52 \pm 0.67$  and  $18.40 \pm 2.23\%$ ) to 600 ppm trees ( $16.95 \pm 0.81\%$ ), then an increase in  $\Delta^{13}\text{C}$  to 800 ppm ( $18.35 \pm 1.73\%$ ) and another

increase to 1000 ppm ( $19.30 \pm 3.30\%$ ). Not only does this data not follow the expected relationship between  $\Delta^{13}\text{C}_{\text{leaf}}$  and  $p\text{CO}_2$ , it is non-monotonic and U-shaped, not following one overall trend. We were hard-pressed to interpret this data, and developed two hypotheses for why we might be observing this strange relationship.

Our first hypothesis was that tree health was obscuring our results. Studies that have shown the expected positive relationship between  $\Delta^{13}\text{C}_{\text{leaf}}$  and  $p\text{CO}_2$  were carried out in extremely well-controlled growth chambers where plant health was minimally variable and overall very good [Schubert and Jahren 2012]. Our experiment has health variability between trees (Figure 19). Stress was not part of the experimental design of this study, but an unintended consequence of bad weather and poor drainage. In order to assess the effect of tree health on  $\Delta^{13}\text{C}_{\text{leaf}}$ , in 2018 we scored each tree on a semi-quantitative 3-point scale, where “1” was the least healthy and “3” the most. We looked at leaf size, color, and curling of leaves (which indicates water stress).



**Figure 19.** A very healthy tree in our experiment on the left, rated a “3” on our health score. A very unhealthy tree on the right, rated a “1” on our health score.



Tree health was found to have an effect on  $\Delta^{13}\text{C}_{\text{leaf}}$  values (Figure 20).  $\Delta^{13}\text{C}_{\text{leaf}}$  increased with health, from an average of 15.28‰ for the trees rated “1” to 19.05‰ for the trees rated “3”. Using our scale, tree health is largely an indicator of water stress on the trees. When plants are water stressed, they conserve water by partially or completely closing the stomata on the bottom of their leaves. This limits water loss, but also prevents  $\text{CO}_2$  from entering the leaf, resulting in a decrease in  $\text{C}_i$  relative to plants that are not stressed. This relative decrease in  $\text{C}_i$  causes a decrease in  $\Delta^{13}\text{C}_{\text{leaf}}$  for plants that are stressed relative to those that are perfectly healthy.

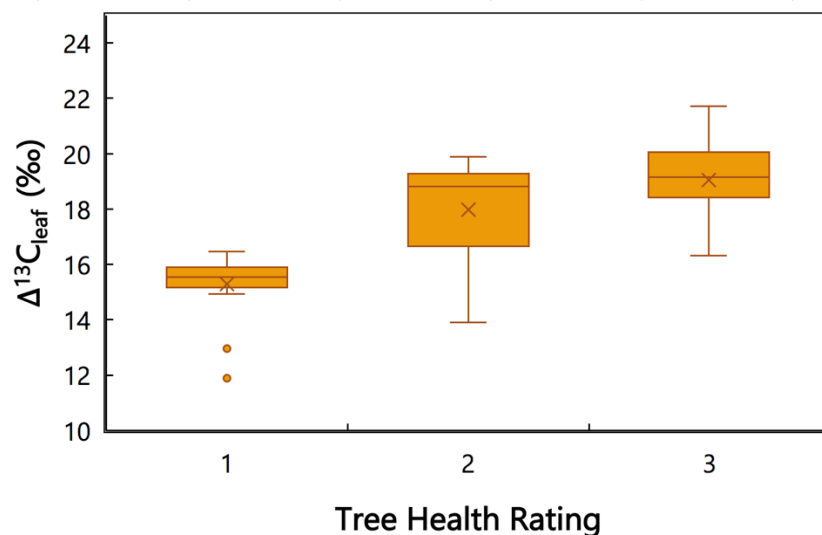


**Figure 20.** Boxplot of  $\Delta^{13}\text{C}_{\text{leaf}}$  values from the last four weeks of the growing season binned by tree health rating. “X”s represent the mean value for each bin.

Though there clearly is a dependence of  $\Delta^{13}\text{C}_{\text{leaf}}$  on health, we did not find that health was changing the overall relationship that we observed between  $\Delta^{13}\text{C}_{\text{leaf}}$  and  $p\text{CO}_2$ . There was at least one extremely healthy tree rated a “3” at each  $\text{CO}_2$  treatment level, and plotting just these healthiest trees’  $\Delta^{13}\text{C}_{\text{leaf}}$  against  $p\text{CO}_2$  showed the same relationship as

the whole dataset (Figure 21). Though stress on the trees does lead to a lower  $\Delta^{13}\text{C}_{\text{leaf}}$ , it does not affect the shape of the relationship that we observed.

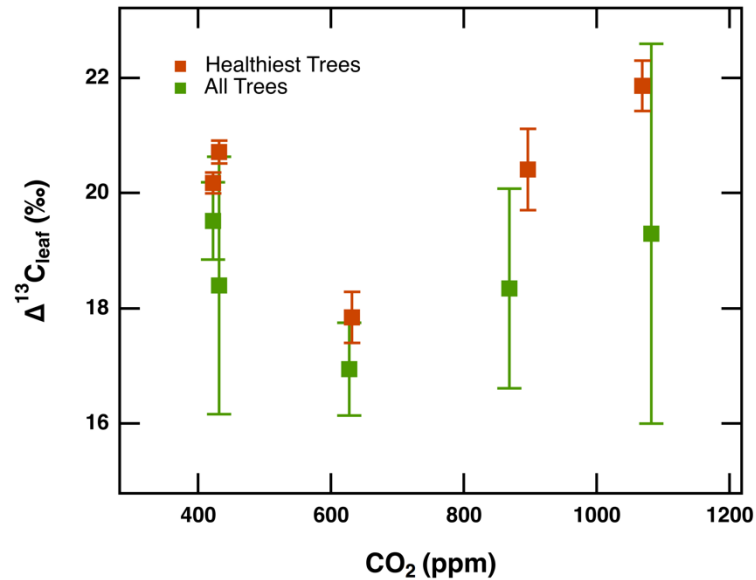


**Figure 21.**  $\Delta^{13}\text{C}_{\text{leaf}}$  of the healthiest trees and all of the trees plotted against  $p\text{CO}_2$ . Red squares represent the average value of all trees at each treatment level, and yellow squares represent the healthiest tree at each level. Error bars represent one standard deviation.

In 2019, we added sapling in pots to the experiment. These saplings were well-watered through the growing season and overall appeared to be extremely healthy. These saplings also helped us to investigate the effect of tree health on  $\Delta^{13}\text{C}_{\text{leaf}}$ , giving us a larger sample size of data to analyze. With this dataset from the saplings (also referred to as “small trees”), we also did not detect an increase in  $\Delta^{13}\text{C}_{\text{leaf}}$  with an increase in  $p\text{CO}_2$  (Figure 23).

After determining that tree health couldn’t explain the relationship that we observed between  $\Delta^{13}\text{C}_{\text{leaf}}$  and  $p\text{CO}_2$ , we investigated our second hypothesis that stored starches were offsetting the  $\Delta^{13}\text{C}_{\text{leaf}}$  values. When leaves begin to grow, they use starch

reserves stored from prior years until leaves develop airspaces and can photosynthesize, fixing carbon from their atmosphere. In other words, leaves begin growing with old carbon and then add new carbon from their environment. If the old carbon is of a different isotopic composition than the new carbon added through photosynthesis, then a measurement of  $\delta^{13}\text{C}_{\text{leaf}}$  would reflect a combination of old and new carbon while we are only interested in the new carbon from elevated  $\text{CO}_2$  atmospheres.

The  $\text{CO}_2$  that we added to experimental atmospheres had a much more negative  $\delta^{13}\text{C}$  value than ambient air (about -40‰ compared to about -10‰), so starches stored prior to being under experimental conditions would result in less negative  $\delta^{13}\text{C}_{\text{leaf}}$  values, they would contain more  $^{13}\text{C}$ . If our trees and their stored starches were not in equilibrium with their experimental atmospheres, the calculated  $\Delta^{13}\text{C}$  from these leaf values would be artificially low. With increasing treatment levels, the elevated  $\text{CO}_2$  atmospheres are increasingly depleted in  $^{13}\text{C}$ , so the effect of stored starches is incrementally larger. If we could remove the effect of stored starches in this scenario, we would expect the average  $\Delta^{13}\text{C}_{\text{leaf}}$  values of the 600, 800, and 1000 ppm trees to go up, giving a positive relationship between  $\Delta^{13}\text{C}_{\text{leaf}}$  and  $p\text{CO}_2$ .

In order to test if stored starches were having an effect on our observed relationship between  $\Delta^{13}\text{C}$  and  $p\text{CO}_2$ , we measured  $\delta^{13}\text{C}$  of leaves from our experimental trees from before they entered experimental conditions (2015) through 2019 (Figure 22). In 2015 before entering the experiment, leaves from different trees had very similar isotopic compositions with an average and standard deviation of  $-28.29 \pm 0.41$ ‰. The trees were put under experimental atmospheres halfway through the growing season in 2016, where we see the composition of the leaves begin to diverge into treatment levels,

with the highest CO<sub>2</sub> trees having the most negative and <sup>13</sup>C depleted values. The treatment groups separated fully after the 2017 season when they had been under experimental atmospheres for one and a half growing seasons. There was a slight increase in  $\delta^{13}\text{C}$  values from 2017 to 2018 and 2018 to 2019 which can be attributed to the trees being under some stress. Overall, after 2017, trees were in equilibrium with their atmospheres, as evidenced by the asymptote in separation of  $\delta^{13}\text{C}_{\text{leaf}}$  values. The small increases in  $\delta^{13}\text{C}$  between 2017 and 2018 and 2018 and 2019 are likely a signal of stress. Overall, trees were more stressed in 2019 than 2018, and 2018 than 2017. As discussed above, stress causes a lower  $\Delta^{13}\text{C}_{\text{leaf}}$  value from an increase in  $\delta^{13}\text{C}$ .

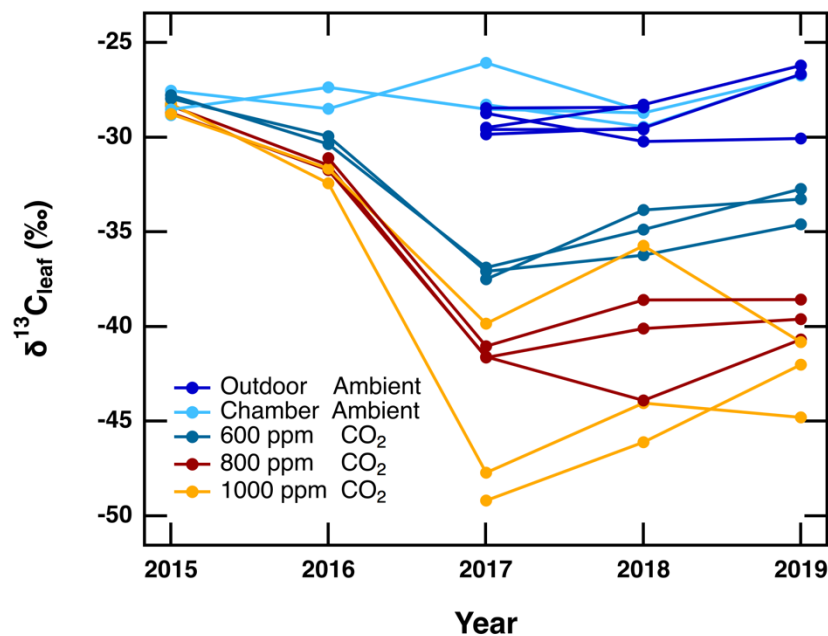


**Figure 22.**  $\delta^{13}\text{C}_{\text{leaf}}$  values from abscised leaves collected in the fall of 2015, 2016, 2017, 2018, and green leaf values from the summer of 2019 plotted against time. Each point represents a  $\delta^{13}\text{C}_{\text{leaf}}$  measurement from one leaf from one tree. Dark blue points represent outdoor ambient trees, light blue represents chamber ambient trees, teal represents 600 ppm trees, red represents 800 ppm trees, and yellow 1000 ppm trees.

We calculated  $\Delta^{13}\text{C}_{\text{leaf}}$  values from leaves collected in 2018 and in 2019, so stored starches would not have an effect on  $\Delta^{13}\text{C}_{\text{leaf}}$  as the trees and their starch reserves were already in equilibrium with their experimental atmospheres. Neither tree health nor stored starches can explain the relationship found in 2018 between  $\Delta^{13}\text{C}_{\text{leaf}}$  and  $p\text{CO}_2$ .

In the 2019 growing season, we again measured  $\Delta^{13}\text{C}_{\text{leaf}}$  from the mature trees as well as the small potted trees that were added to chambers in the spring of 2019. This data is shown in Figure 23. Again, it is clear that we do not see an increase in  $\Delta^{13}\text{C}_{\text{leaf}}$  with an increase in  $p\text{CO}_2$ . However, we do not see the same U-shaped relationship that we observed in 2018. Instead, there is more of a general downward trend in  $\Delta^{13}\text{C}_{\text{leaf}}$  with  $p\text{CO}_2$ . The  $\Delta^{13}\text{C}_{\text{leaf}}$  values from the small trees are all higher than the mature trees, with offsets ranging from 0.26‰ for the outdoor ambient trees to 2.73‰ for the 800 ppm trees. The higher  $\Delta^{13}\text{C}_{\text{leaf}}$  values for the small trees are again likely due to the effect of stress: the small trees were able to be watered more completely than mature trees and the soil is loamier, so less water stress means stomata can stay open and  $C_i$  does not decrease.

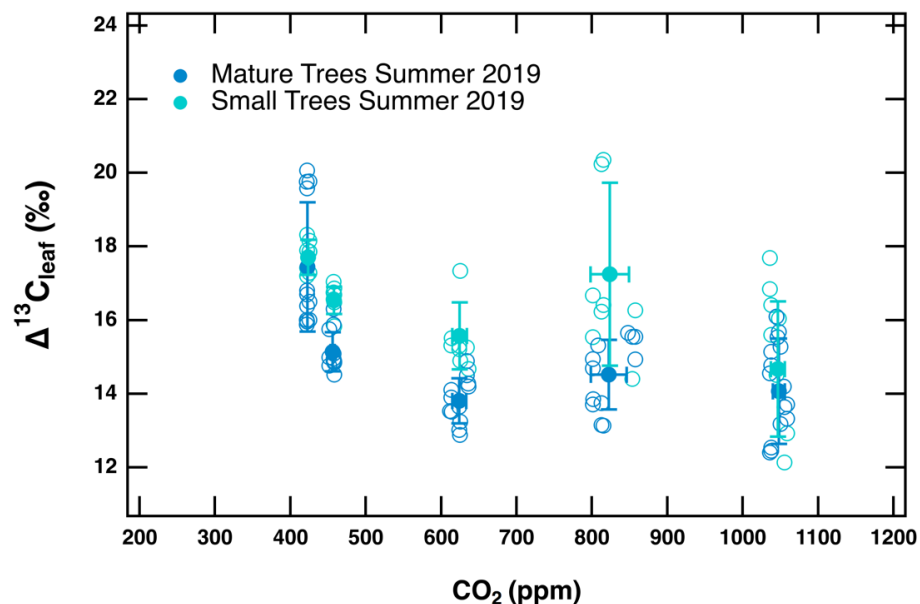


**Figure 23.**  $\Delta^{13}\text{C}_{\text{leaf}}$  values from the last four weeks of the 2019 growing season for both mature (dark blue) and small (light blue) trees. Open circles represent individual leaves. Filled circles represent the average  $\Delta^{13}\text{C}_{\text{leaf}}$  value for each treatment level. Horizontal error bars represent one standard deviation in the actual  $[\text{CO}_2]$  of each chamber, and vertical one standard deviation of  $\Delta^{13}\text{C}_{\text{leaf}}$  values.

When we look at all three datasets (2018 mature trees, 2019 mature trees, 2019 small trees) together, there is no easy relationship to draw from Figure 24. The U-shaped relationship from mature trees in 2018 was not completely replicated by mature trees or small trees in 2019. From the combined data, there appears to be either no relationship or a negative relationship between  $\Delta^{13}\text{C}_{\text{leaf}}$  and  $p\text{CO}_2$  over 400 to 1000 ppm  $\text{CO}_2$ , though there seems to be a repeated decrease in  $\Delta^{13}\text{C}_{\text{leaf}}$  between ambient trees and 600 ppm trees in all three datasets. Above 600 ppm, the response of  $\Delta^{13}\text{C}_{\text{leaf}}$  to increasing  $p\text{CO}_2$  varies.

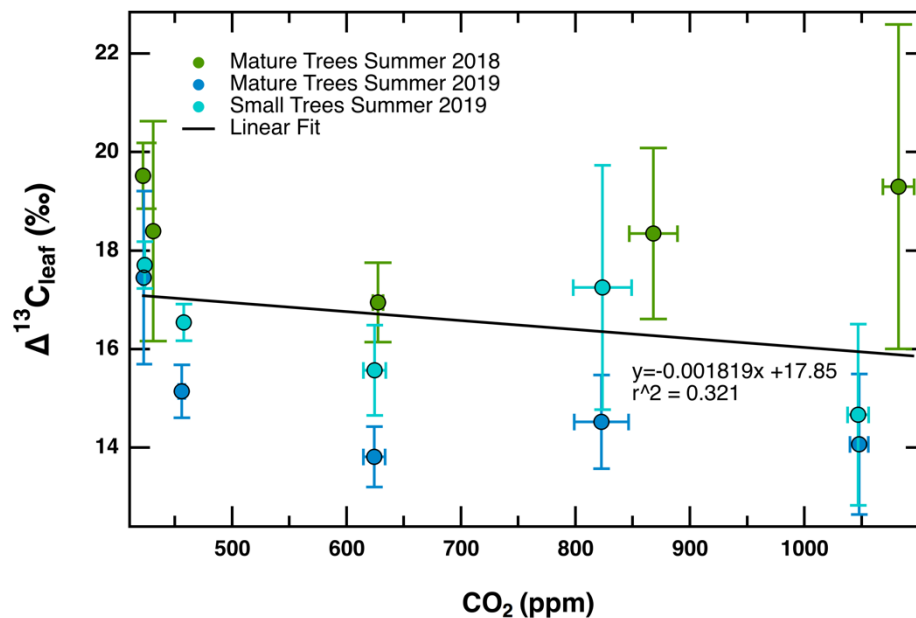


**Figure 24.**  $\Delta^{13}\text{C}_{\text{leaf}}$  values from the last four weeks of the 2018 season for mature trees (green) and the 2019 growing season for both mature (dark blue) and small (light blue) trees. Filled circles represent the average  $\Delta^{13}\text{C}_{\text{leaf}}$  value for each treatment level. Horizontal error bars represent one standard deviation in the actual  $[\text{CO}_2]$  of each chamber, and vertical one standard deviation of  $\Delta^{13}\text{C}_{\text{leaf}}$  values. Linear fit through all data gives  $y = -0.001819x + 17.85$  with an  $r^2$  of 0.321.

### ***Discussion***

Our results suggest a negative/no relationship between  $\Delta^{13}\text{C}_{\text{leaf}}$  and  $p\text{CO}_2$  which is at odds with the relationship found in Schubert and Jahren 2012. There are important differences between our study and theirs: (1) This study is of a single tree species, *G. biloba*, while Schubert and Jahren studied two small annual plants *R. sativus* and *A. thaliana*. (2) Soil moisture and relative humidity varied naturally in our study. In Schubert and Jahren 2012, both of these variables were extremely well-controlled for consistent soil moisture and relative humidity (40%).

Schubert and Jahren created a compilation of 11 studies that they used to support the relationship that they found in *R. sativus* and *A. thaliana*. Different species exhibit different offsets in carbon isotopic compositions and therefore  $\Delta^{13}\text{C}_{\text{leaf}}$  values, so a plot of  $\Delta^{13}\text{C}_{\text{leaf}}$  versus  $p\text{CO}_2$  can be confusing. Two species may show the same relationship, but be offset by several ‰. To assess multiple sets of  $\Delta^{13}\text{C}_{\text{leaf}}$  versus  $p\text{CO}_2$  data without the offsets that exist between species, sensitivity (S) can be used to normalize data.

Sensitivity is the first derivative of a  $\Delta^{13}\text{C}_{\text{leaf}}$  versus  $p\text{CO}_2$  plot, it is calculated by Equation 11:

$$\text{Sensitivity } (\text{‰}/\text{ppm}) = \frac{d(\Delta^{13}\text{C})}{d(p\text{CO}_2)} \quad (11)$$

When sensitivity is positive, it indicates an increase in  $\Delta^{13}\text{C}_{\text{leaf}}$  with  $p\text{CO}_2$ . When sensitivity is negative, it indicates a decrease in  $\Delta^{13}\text{C}_{\text{leaf}}$  with  $p\text{CO}_2$ . Figure 25 is a reproduction of Figure 3 from Schubert and Jahren 2012. It shows sensitivity values versus  $\text{CO}_2$ . Each data point represents a calculated sensitivity value from two

discrimination data points:

$$\text{Sensitivity } (\text{‰}/\text{ppm}) = \frac{\Delta^{13}\text{C}_{\text{high}} - \Delta^{13}\text{C}_{\text{low}}}{p\text{CO}_{2\text{high}} - p\text{CO}_{2\text{low}}} \quad (12)$$

The calculated sensitivity is plotted against the average of the two  $p\text{CO}_2$  values. The error bars extend to the lower and the upper  $p\text{CO}_2$  values. This data was fit with a hyperbolic curve, showing very large positive sensitivity values at low levels of  $\text{CO}_2$  that asymptote to low positive sensitivity values at high  $\text{CO}_2$ . The high sensitivity at low  $p\text{CO}_2$  (<1000 ppm) indicates that the C3 plant proxy would be useful in this range, but likely not above ~1000 ppm, because as large changes in  $p\text{CO}_2$  would yield only minimal changes in  $\Delta^{13}\text{C}_{\text{leaf}}$ . It is expected that at a certain level of  $p\text{CO}_2$ , this response would asymptote as RuBisCO becomes saturated with  $\text{CO}_2$ .



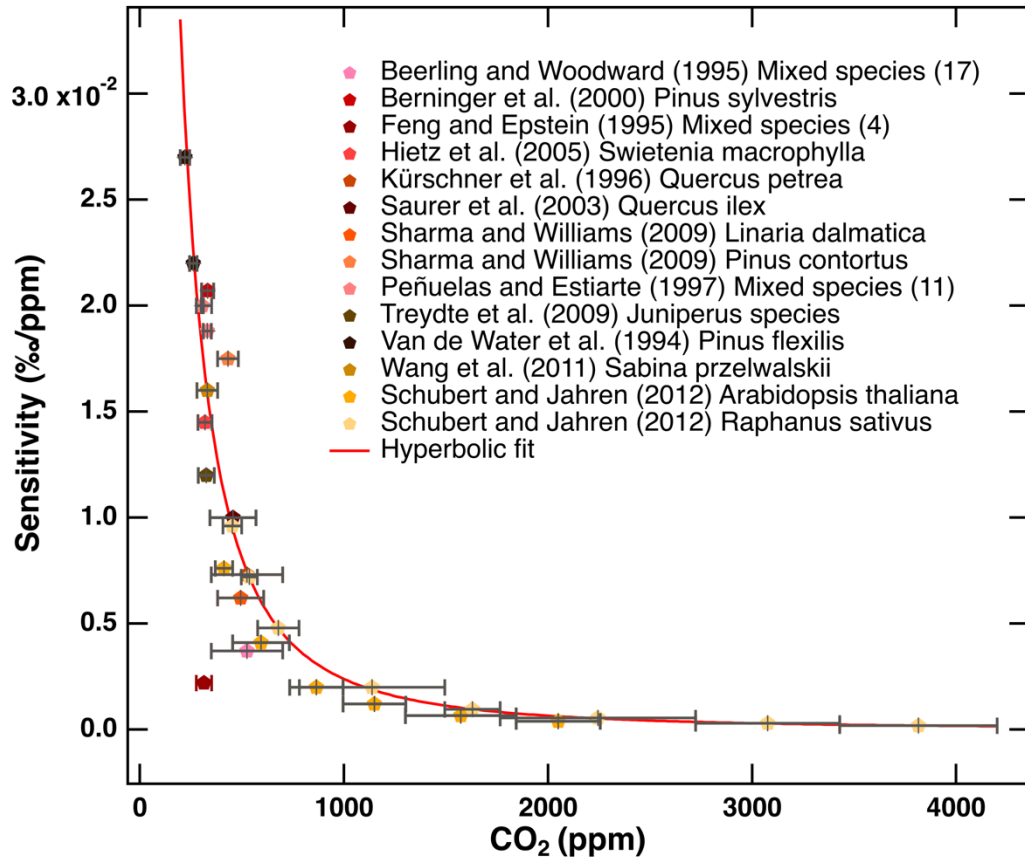


**Figure 25.** Reproduced from Figure 3 in Schubert and Jahren 2012. Sensitivity is plotted against  $\text{CO}_2$  for a variety of studies, listed in the legend. The pentagon is located on the average  $\text{CO}_2$  for two treatment levels. The errors bars represent the span of  $\text{CO}_2$  that the two treatments cover. The red line through the data is a hyperbolic fit:  

$$S = (0.21)(28.26)^2 / [28.26 + 0.21(p\text{CO}_2 + 250)]^2.$$

The data from this study (Figure 26, *Ginkgo biloba*) shows a very different relationship than Schubert and Jahren 2012. Overall, this sensitivity plot shows almost the exact opposite relationship (mirror over the x-axis) as the Schubert and Jahren compilation. Rather than decreasing from positive sensitivity to zero, we see increasing negative sensitivity to zero. All sensitivity values are negative aside from a few values at 600 and 800 ppm, and even these are very close to zero. The largest decrease in  $\Delta^{13}\text{C}_{\text{leaf}}$  with  $p\text{CO}_2$  was from outdoor ambient trees to chamber ambient trees, then from chamber

ambient trees to 600 ppm trees (Figure 26). Our results are clearly not in agreement with Schubert and Jahren's compilation.

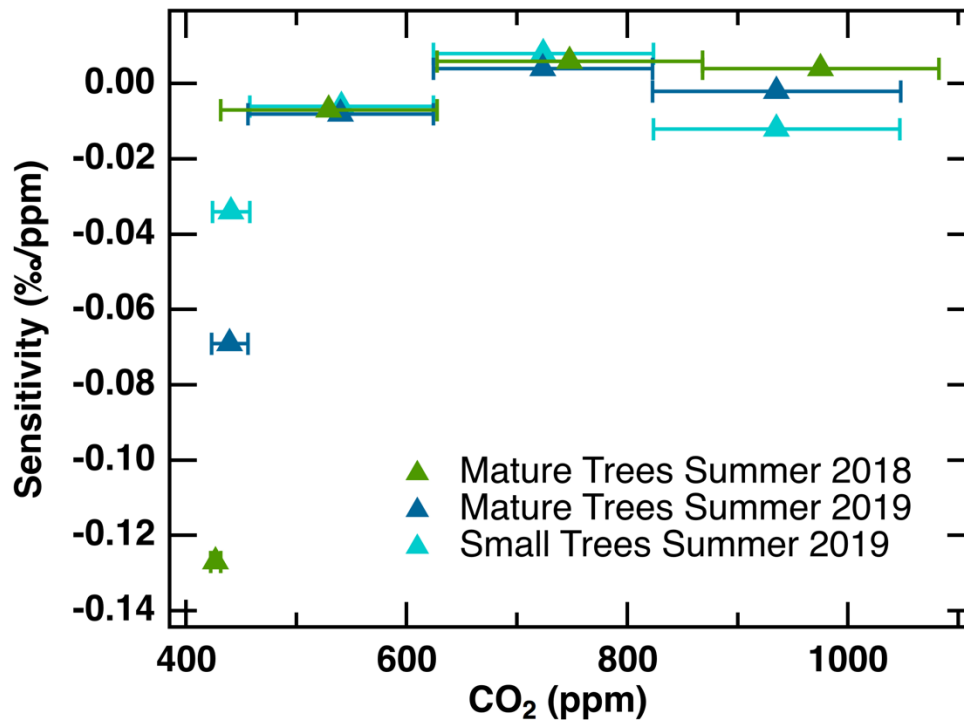


**Figure 26.** Sensitivity values calculated from this study. The triangle is located on the average CO<sub>2</sub> for two treatment levels. The errors bars represent the span of CO<sub>2</sub> that the two treatments cover. Colors indicate the dataset. Light blue – small trees 2019, dark blue- mature trees 2019, green- mature trees 2018.

Schubert and Jahren's compilation (Figure 25) showed a striking, well-defined relationship that would be useful in paleo-CO<sub>2</sub> reconstructions. To understand why our *G. biloba* data does not agree with this curve, two main issues with the Schubert Jahren compilation will be discussed: (1) In order to attain the sensitivity values from the published datasets that they cite, large groups of data from multiple species was sometimes averaged with no regard to a mix of responses within that average. In studies that contained multiple species that showed very different responses, all of the responses were averaged together. Some of the values were either miscalculated or misreported. (2)

This compilation purposefully excluded data that did not support a positive relationship between  $\Delta^{13}\text{C}_{\text{leaf}}$  and  $p\text{CO}_2$ .

Following issue (1), data from 17 species at three levels of  $p\text{CO}_2$  from Beerling and Woodward 1995 was combined into just one data point in Figure 25. If the data from the original paper is broken down into each species and into two S values rather than combined into one, the sensitivity versus  $p\text{CO}_2$  plot looks like Figure 27. From this figure, we see that there are a variety of responses to increasing  $p\text{CO}_2$  among the different species of plant present. While the majority of S values are positive, almost one-third (11 out of 34) are negative. Clearly, there are species-specific responses that are ignored when all of this data is combined into one data point in the Schubert and Jahren compilation (2012).

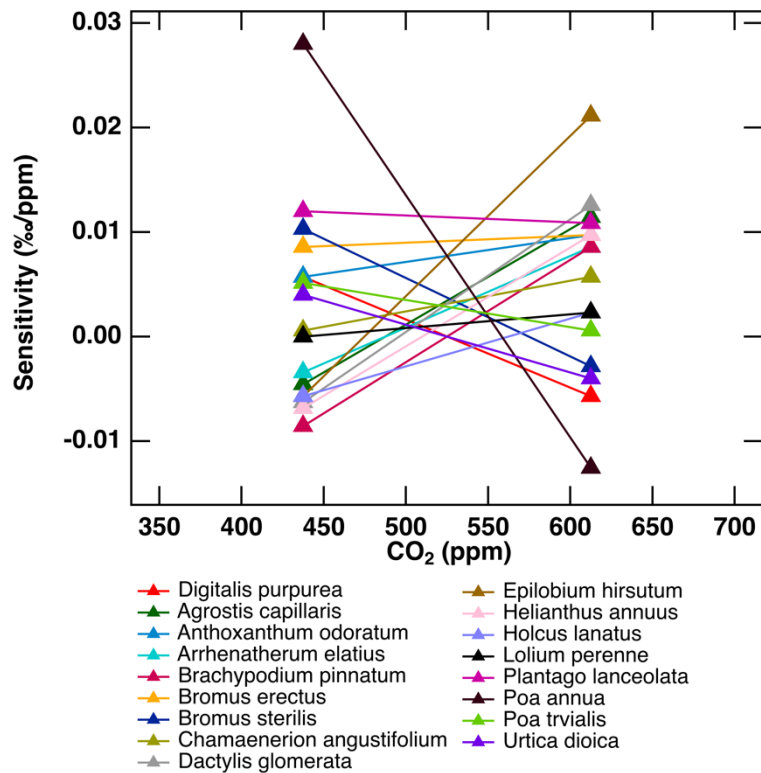


**Figure 27.** Sensitivity values from Beerling and Woodward 1995, calculated from raw data. Sensitivity is plotted against  $\text{CO}_2$  for a variety of species (17). The triangle is

located on the average CO<sub>2</sub> for two treatment levels. Lines were added connecting points from the same species. S values at 438 ppm are from experiments at 350 and 525 ppm. S values at 613 ppm are from experiments at 525 and 700 ppm.

Data from Hietz et al. 2005 was used in Schubert and Jahren's compilation for an S value of 0.0145 ‰/ppm for *Swietenia macrophylla*, a positive relationship between  $\Delta^{13}\text{C}_{\text{leaf}}$  and  $p\text{CO}_2$ . However, when the original  $\Delta^{13}\text{C}_{\text{leaf}}$  data from the paper is digitized and plotted against  $p\text{CO}_2$  (data from <https://data.giss.nasa.gov/modelforce/ghgases/fig1A.ext.txt>), there is actually a *negative* relationship between  $\Delta^{13}\text{C}_{\text{leaf}}$  and  $p\text{CO}_2$  (Figure 28). From this plot, the *S. macrophylla* data gives an S value of -0.013 ‰/ppm when a linear fit is used to calculate S. Schubert and Jahren's compilation also ignores the *Cedrela odorata* data which gives another negative S value of -0.003 ‰/ppm when a linear fit is used to calculate S. The *S. macrophylla* data was either miscalculated or misreported, while the *C. odorata* data was ignored, following point (2). While some of the raw data present in this compilation can reproduce the values that Schubert and Jahren used, there is clearly data that is used incorrectly.

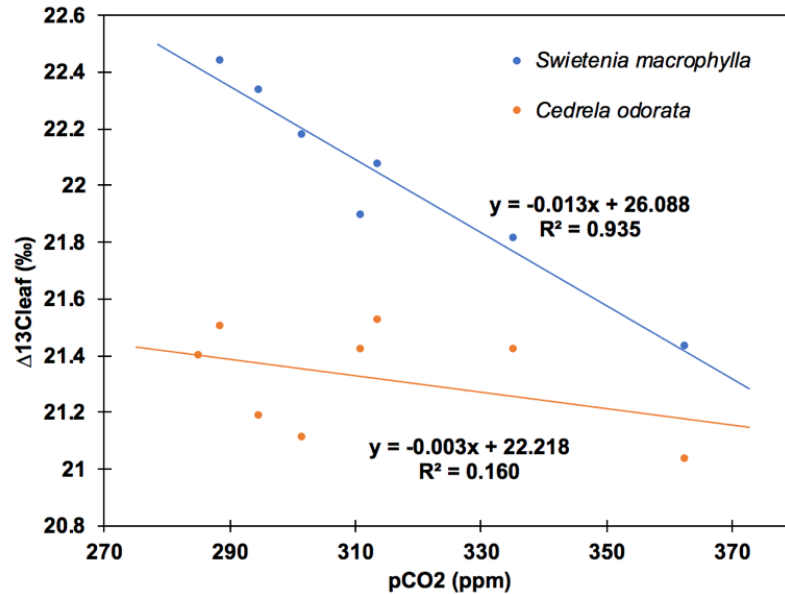


**Figure 28.**  $\Delta^{13}\text{C}_{\text{leaf}}$  data from Hietz et al. 2005 plotted against  $p\text{CO}_2$  (data from <https://data.giss.nasa.gov/modelforce/ghgases/fig1A.ext.txt>). Both datasets (*S. macrophylla*, blue and *C. odorata*, orange) show decreasing trends in  $\Delta^{13}\text{C}_{\text{leaf}}$  with  $p\text{CO}_2$  (linear fit).

Aside from the Hietz et al. data (2005), there are other studies (including our study) that have found either no relationship or a negative relationship between  $\Delta^{13}\text{C}_{\text{leaf}}$  and  $p\text{CO}_2$  (Hietz et al. 2005; Tu et al. 2004; Peñuelas and Azcón-Bieto 1992; Lomax et al. 2019). Like the Schubert and Jahren 2012 compilation, these studies also include a variety of species and include studies that are geological, use herbarium sheets, and are experimental with growth chambers.

Using mature modern oak trees and Miocene fossil oak of two ages, Tu et al. (2004) investigated discrimination for whole leaves. Experimental *Quercus petraea* trees were at 350 and 700 ppm, a ‘nature’ tree at 370 ppm, and Miocene fossils (*Quercus psuedocastanea*) from 2 ages known to be 280 and 360 ppm. Fossil leaves had a smaller discrimination overall than modern, but there was no overall significant effect of  $p\text{CO}_2$  on discrimination found. Sensitivity values from this study (Figure 29) show that there is

no consistent relationship, with negative S values at the low and high ends of CO<sub>2</sub> treatment and positive values (spanning small increments of pCO<sub>2</sub>) in the middle.

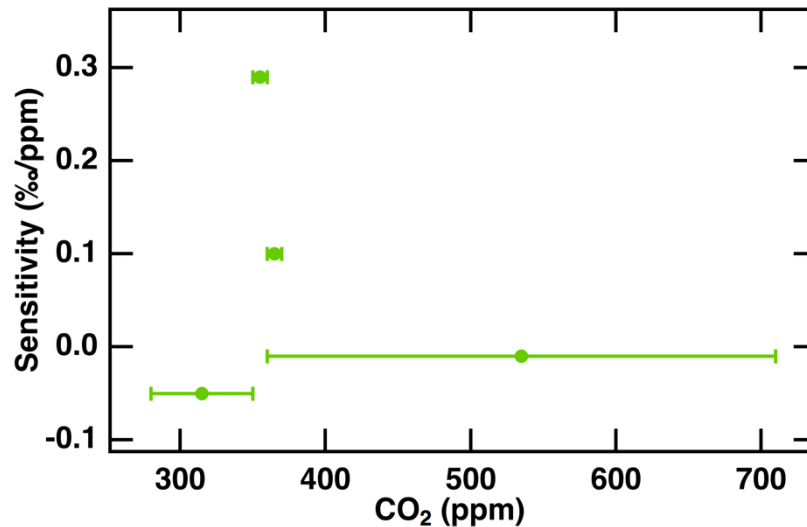


**Figure 29.** Sensitivity values calculated from Tu et al. 2004. Circles The triangle is located on the average CO<sub>2</sub> for two treatment levels. The horizontal error bars represent the span of CO<sub>2</sub> that the two treatments cover.

Peñuelas and Azcón-Bieto (1992) used herbarium specimens to study changes in  $\Delta^{13}\text{C}_{\text{leaf}}$  over historical CO<sub>2</sub> change from 280 to 348 ppm (1750-1988). The 12 species studied are endemic to a Mediterranean climate. Their data shows a variety of responses to pCO<sub>2</sub>. 21 of the 36 sensitivity values plotted in Figure 30 are negative. Of the 21 species, only 2 (*Alnus glutinosa* and *Hellebores foetidus*) showed a consistent relationship between S and pCO<sub>2</sub>, both of which consistently decreased in sensitivity with increasing pCO<sub>2</sub>. *A. glutinosa* decreased from 0.042 ‰/ppm to 0.0165 ‰/ppm, indicating a relationship similar to Schubert and Jahren (2012) where an increase in pCO<sub>2</sub> causes an increasingly small increase in  $\Delta^{13}\text{C}_{\text{leaf}}$ . *H. foetidus* decreased from 0.11‰/ppm to -0.0165 ‰/ppm. Though S decreases with increasing pCO<sub>2</sub>, this relationship does not support Schubert and Jahren (2012). At low CO<sub>2</sub>, *H. foetidus* shows an increase in  $\Delta^{13}\text{C}_{\text{leaf}}$  with

an increase in  $p\text{CO}_2$ , but at higher  $\text{CO}_2$ , *H. foetidus* showed a decrease in  $\Delta^{13}\text{C}_{\text{leaf}}$  with an increase in  $p\text{CO}_2$ . The changing direction of the relationship for *H. foetidus* makes it either useless for the C3 plant proxy which relies on decreasing positive S over increasing  $p\text{CO}_2$ , or useful only under a certain level of  $p\text{CO}_2$ . All other species studied by Peñuelas and Azcón-Bieto show changing responses as well. Only one species from this study (*A. glutinosa*) supports a positive relationship between  $\Delta^{13}\text{C}_{\text{leaf}}$  and  $p\text{CO}_2$ , all others (11) do not.

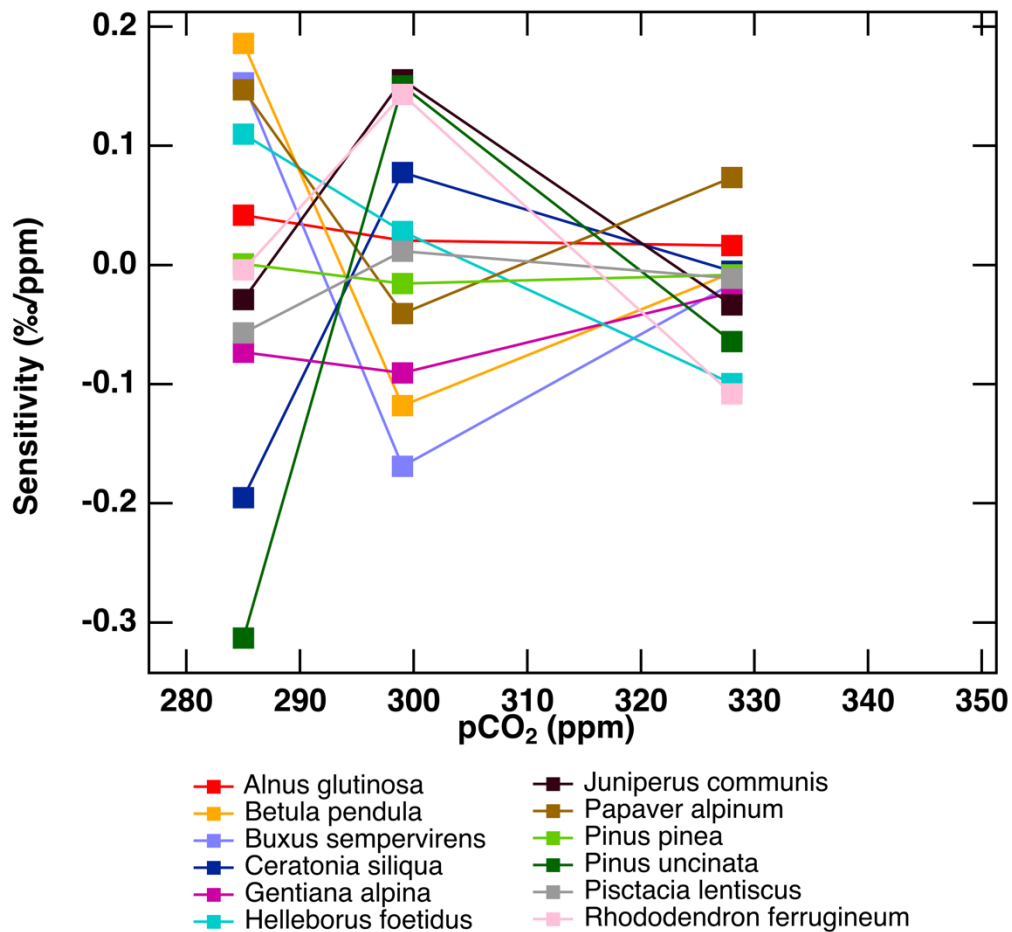


**Figure 30.** Sensitivity values calculated from Peñuelas et al. 1992. The square is located on the average  $\text{CO}_2$  for two treatment levels. Lines were added connecting points from the same species. S values at 285 are from periods of 280 and 290 ppm  $\text{CO}_2$ , S values at 299 are from periods of 290 and 308 ppm, S values at 328 are from periods of 308 and 348 ppm.

Lomax et al. (2019) studied one of same species as Schubert and Jahren did in their 2012 work, *Arabidopsis thaliana*. These plants were also grown in well-controlled growth chambers, at 6 levels of  $p\text{CO}_2$  ranging from 380 to 3000 ppm. After 4 weeks of growth, plants were subjected to one of 3 watering regimes (10 mL per day per pot, 20 mL per day per pot, or permanently saturated) for 2 weeks before being harvested. The results showed a large spread in response to  $p\text{CO}_2$  that isn't clearly explained by difference in watering regimes. From the sensitivity plot below (Figure 31), there is no clear trend in sensitivity on the whole, or between watering regimes. S values show a changing response (positive to negative or vice-versa) for every watering regime. This work was not able to reconstruct the same relationship as Schubert and Jahren observed for *A. thaliana* (2012), and also showed that watering regime introduces additional variability to the relationship between  $\Delta^{13}\text{C}_{\text{leaf}}$  and  $p\text{CO}_2$ .

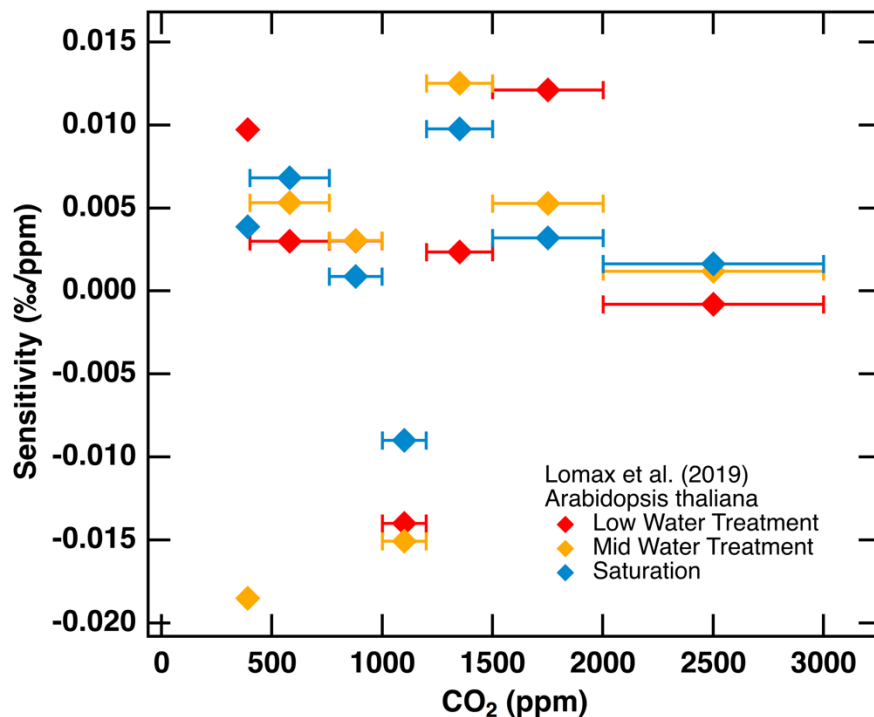




**Figure 31.** Sensitivity values calculated from Lomax et al. 2019. The square is located on the average CO<sub>2</sub> for two treatment levels. The errors bars represent the span of CO<sub>2</sub> that the two treatments cover. Colors indicate watering regime: red is low water treatment, yellow is mid water treatment, and blue is saturated water treatment.

These major flaws in Schubert and Jahren's compilation ((1) misuse of published studies and (2) exclusion of contrary studies) are significant and show that their relationship between  $\Delta^{13}C_{leaf}$  and  $pCO_2$  cannot be applied to all species, and can sometimes not even be applied to the same species (in the case of Lomax et al.'s study of *A. thaliana*). In addition to these flaws, their relationship is also problematic because of: (3) restriction of application because of empirical fitting parameters, (4) differences in the fractionation due to RuBisCO in different species, and (5) stomatal control in different watering regimes and with differing leaf-gas exchange strategies.

The relationship found by Schubert and Jahren is used to reconstruct paleo-CO<sub>2</sub> by looking at relative changes in  $\Delta^{13}C$  over time, following equation 12 (Cui and Schubert 2016).

$$\Delta(\Delta^{13}C) = \Delta^{13}C_{(t)} - \Delta^{13}C_{(t=0)} \quad (13)$$

Where  $\Delta^{13}C_{(t)}$  is the  $\Delta^{13}C$  at the time of interest and  $\Delta^{13}C_{(t=0)}$  is the  $\Delta^{13}C$  at a known time of known  $pCO_2$  and  $\Delta^{13}C$ .  $\Delta(\Delta^{13}C)$  is solved for, and the empirical fitting parameters (Equation 14) of the hyperbolic relationship between  $\Delta^{13}C_{leaf}$  and  $pCO_2$  are plugged in to solve for  $pCO_{2(t)}$ ,  $pCO_2$  at the time of interest, following Equation 15.

$$\Delta^{13}C_{leaf} = \frac{(A)(B)(pCO_2+C)}{(A)+(B)(pCO_2+C)} \quad (14)$$

$$pCO_{2(t)} = \frac{\Delta(\Delta^{13}C) * A^2 + \Delta(\Delta^{13}C) * A * B * pCO_{2(t=0)} + 2 * \Delta(\Delta^{13}C) * A * B * C + \Delta(\Delta^{13}C) * B^2 * C * pCO_{2(t=0)} + \Delta(\Delta^{13}C) * B^2 * C^2 + A^2 * B * pCO_{2(t=0)}}{A * B^2 - \Delta(\Delta^{13}C) * A * B - \Delta(\Delta^{13}C) * B^2 * pCO_{2(t=0)} - \Delta(\Delta^{13}C) * B^2 * C} \quad (15)$$

Clearly, the fitting parameters of the hyperbolic relationship are quite important in the determination of  $pCO_{2(t)}$ . The value of “A” in Equation 14 determines the asymptote of  $\Delta^{13}C$  values, and the combination of values is such that at 0 ppm,  $\Delta^{13}C=4.4\%$ , the fractionation from stomatal diffusion alone (Schubert and Jahren 2012).

Lomax et al. (2019) found that using the C3 plant proxy with the relationship in Equation 14 makes it impossible to apply the proxy to values of  $\Delta^{13}C_{\text{leaf}}$  that are above those of the empirical fitting parameter “A”. Schubert and Jahren set the preferred value of “A” at 28.26, so if any plants exhibit a  $\Delta^{13}C$  value higher than 28.26‰, the model does not work. Lomax et al. found this to occur within their own study of *A. thaliana* (one of the same species studied by Schubert and Jahren that created this curve) nine times. When there is a  $\Delta^{13}C_{\text{leaf}}$  value over 28.26 (the value of fitting parameter “A”) it is impossible to apply the hyperbolic relationship and predict paleo- $CO_2$ . The value of “A” then limits this proxy to plants that don’t have high values of  $\Delta^{13}C$ , which puts the underlying mechanism of the relationship put forth by Schubert and Jahren into question.

While the fractionation by RuBisCO is largely treated as a constant, different species have slightly different version of RuBisCO, causing differences in fractionation through carbon fixation. RuBisCO fixes both  $CO_2$  and  $O_2$ , with  $CO_2$  fixation being beneficial for the plant and  $O_2$  fixation causing respiration. RuBisCO’s are optimized for the  $CO_2:O_2$  that they operate under. Under low  $CO_2:O_2$  ratios, RuBisCO’s operates more slowly with a higher activation energy, giving larger fractionation than RuBisCO’s that

are optimized to high CO<sub>2</sub>:O<sub>2</sub> ratios (Tcherkez 2006). Therefore, if different plant species evolved under varying CO<sub>2</sub>:O<sub>2</sub> ratios, the fractionation associated with RuBisCO would vary. This value of “b” in Equation 7 should not be a constant. The value of “A” in Equation 12 also cannot then be applied to other species: “A” controls the maximum value of  $\Delta^{13}\text{C}$ , and following Equation 7 the maximum value of  $\Delta^{13}\text{C}$  is equal to the fractionation from RuBisCO (“b”) as  $C_i/C_a$  cannot exceed 1.

The C3 plant proxy is reliant upon stomata opening more with an increase in  $p\text{CO}_2$ , causing  $C_i$  to increase relative to  $C_a$  for an increased  $\Delta^{13}\text{C}_{\text{leaf}}$  value (Equation 7). If stomata close or remain slightly opened,  $C_i/C_a$  will either remain constant or decrease, giving a null or negative response with increasing  $p\text{CO}_2$ . In *Ginkgo*, we see a decrease in  $\Delta^{13}\text{C}_{\text{leaf}}$  with increasing  $p\text{CO}_2$ , suggesting that stomata are closing to conserve water rather than opening to accept more CO<sub>2</sub>. This physiological response was discussed by Voelker et al. (2016). Plants can utilize several different strategies to regulate their gas exchange (CO<sub>2</sub> in and H<sub>2</sub>O out): (1) maintain a constant  $C_i$ , (2) maintain a constant  $C_a - C_i$ , (3) maintain a constant  $C_i/C_a$ , or (4) a mix of strategies depending whether the ‘goal’ of the plant is to maximize carbon gain, minimize H<sub>2</sub>O loss, or sit somewhere in the middle. Figure 32 shows these strategies and what they look like plotted against  $C_a$ . Panel (c) on figure 32 is the most important for the discussion of  $\Delta^{13}\text{C}_{\text{leaf}}$  and  $p\text{CO}_2$ , as  $C_i/C_a$  is directly proportional to  $\Delta^{13}\text{C}_{\text{leaf}}$  (Equation 6) and  $C_a$  is analogous to  $p\text{CO}_2$ , so panel (c) is analogous to  $\Delta^{13}\text{C}_{\text{leaf}}$  versus  $p\text{CO}_2$  plot. The only leaf-gas exchange strategy that results in the hyperbolic relationship observed by Schubert and Jahren is maintaining a constant  $C_a - C_i$ . With this strategy, carbon gain is valued over water loss. Schubert and Jahren kept the

*A. thaliana* and *R. sativus* plants well-watered, so water stress was not an issue for these plants, and they could afford to lose water for carbon gain.

The relationship exhibited by *Ginkgo* in our study suggests a leaf-gas exchange strategy of a constant  $C_i$ , as the shape of our  $\Delta^{13}C_{\text{leaf}}$  versus  $p\text{CO}_2$  plot matches that of a constant  $C_i$  from panel (c) in figure 32. This is a much more conservative strategy: with increasing  $C_a$ , stomata don't open further to take advantage of increasing carbon gain and are able to instead conserve water while incorporating the same amount of carbon as at a lower  $C_a$ . The *Ginkgo* trees in our study did experience water stress, so it makes sense that they would seek to limit water loss. The difference in leaf-gas exchange strategy between our study and Schubert and Jahren's could be due to more than just watering regime. Plant growth strategy may have influence over leaf gas-exchange strategy. Small herbaceous annual plants may weigh carbon gain for growth over water loss, and large woody trees may weigh water retention over carbon gain and growth.

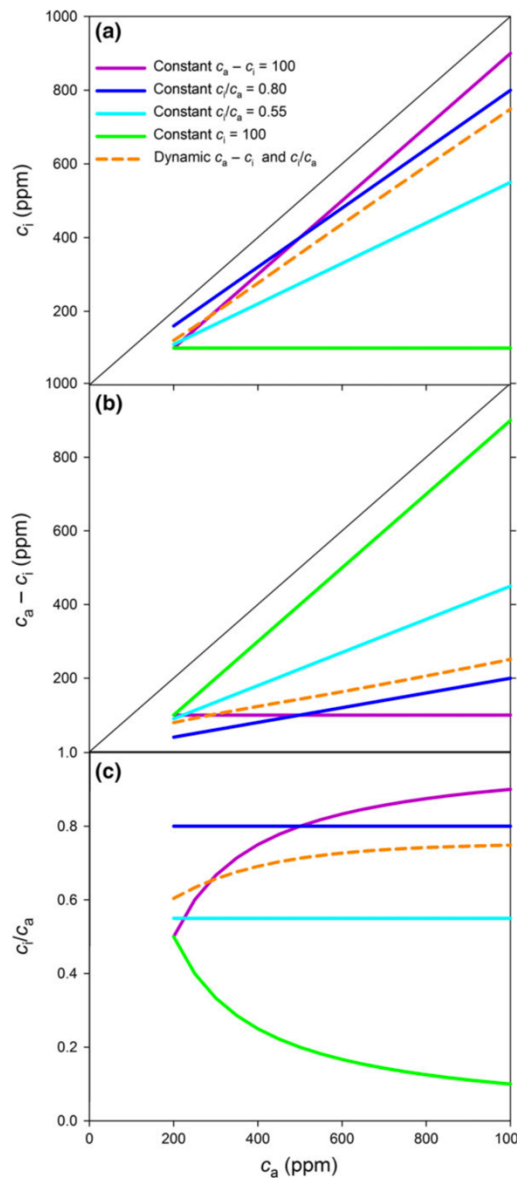


**Figure 32.** Figure 1, Voelker et al. 2016. Leaf gas-exchange strategies plotted as  $C_i$  against  $C_a$  (panel a),  $C_a - C_i$  against  $C_a$  (panel b), and  $C_i/C_a$  (panel c). Each colored curve represents a different leaf gas-exchange stomatal control strategy (refer to legend).

In order to actually measure the gas-exchange strategy of plants, physiological measurements are made. For the past two summers, physiological measurements have been made on the ginkgo trees in our study. With later analysis of this data and of physiological data from other studies that also measured  $\Delta^{13}\text{C}_{\text{leaf}}$ , we will be able to determine the strategy used by *Ginkgo* and other species. Then, we can determine if leaf-gas exchange strategy can explain the difference in  $\Delta^{13}\text{C}_{\text{leaf}}$  responses to  $p\text{CO}_2$  that have

already been discussed. This work is outside confines of this study, but will be important in understanding how  $\Delta^{13}\text{C}_{\text{leaf}}$  varies with  $p\text{CO}_2$ .

Though the above complications (3, 4, and 5) are well-documented, Schubert and Jahren proceeded to apply the positive hyperbolic relationship between  $\Delta^{13}\text{C}_{\text{leaf}}$  and  $p\text{CO}_2$  in *R. sativus* and *A. thaliana* in their 2012 paper to the fossil record (Schubert and Jahren 2015) seemingly without serious regard to several confounding factors. In this paper, total organic matter (TOM) and fossil leaf (*Salix* and *Pinus*)  $\Delta^{13}\text{C}$  data was used to reconstruct  $p\text{CO}_2$  through the last glacial maximum (LGM). They found that the reconstructions from both TOM and leaves matched ice core records very well. This reconstruction has been put under scrutiny. Kohn (2016) points out that the agreement between TOM and ice core  $p\text{CO}_2$  records could be due not to a  $p\text{CO}_2$  response in  $\Delta^{13}\text{C}$ , but rather to a change through the LGM in the abundance of C3/C4 grasses. Schubert and Jahren claim to have removed the possibility of this mixing by only using records that have  $\delta^{13}\text{C}_{\text{leaf}}$  values between -18.5 and -32‰, the range for C3 plants. C4 plants range from -9 to -19‰ (O’Leary 1988). TOM records can be a combination of signals from a variety of plants, so it is impossible to say that a TOM sample with a value between -18.5 and -32‰ is purely a C3 plant record. This  $p\text{CO}_2$  reconstruction is then faulty as the proxy used to create this reconstruction cannot be applied to C4 plants.

Additionally, the TOM and fossil leaf records from this 2015 paper were not specifically from extremely wet environments, against the recommendation that they themselves made in their 2012 paper. It is then impossible to say whether the changes in  $\Delta^{13}\text{C}$  used to reconstruct paleo- $\text{CO}_2$  in this study are due to changes in  $p\text{CO}_2$  or changes in mean annual precipitation (MAP) or humidity. Species-specific responses were also

not considered: the TOM record includes an unknown number and type of C3 plant species, which can all have isotopic varying responses to  $p\text{CO}_2$  because of a difference in stomatal control or a difference in RuBisCo and therefore degree of change in  $\Delta^{13}\text{C}$  with a change in  $p\text{CO}_2$ . The leaf record splices two species together (*Pinus* and *Salix*) which are also prone to the differences that apply to the TOM record.

In short, the relationship between  $\Delta^{13}\text{C}_{\text{leaf}}$  and  $p\text{CO}_2$  is not as simple as it is presented by Schubert and Jahren (2012). This relationship is influenced by a variety of factors, including fitting parameters, differences in RuBisCO fractionation, leaf gas-exchange strategy, and watering regime. While some studies support a positive relationship between  $\Delta^{13}\text{C}_{\text{leaf}}$  and  $p\text{CO}_2$ , others enumerated here oppose that observation (Hietz et al. 2005; Tu et al. 2004; Peñuelas and Azcón-Bieto 1992; Lomax et al. 2019).

When studies the studies discussed above are compiled (Figure 33), the sensitivity plot looks much more complicated than the sensitivity plot of the compilation put forward by Schubert and Jahren (2012) (Figure 25). There is no relationship to be drawn from this plot, other than that there are a range in responses to  $p\text{CO}_2$  at low values (<500 ppm) and that values converge around zero, or no response, above 500 ppm  $\text{CO}_2$ . This kind of relationship is not useful for a paleo- $\text{CO}_2$  proxy.

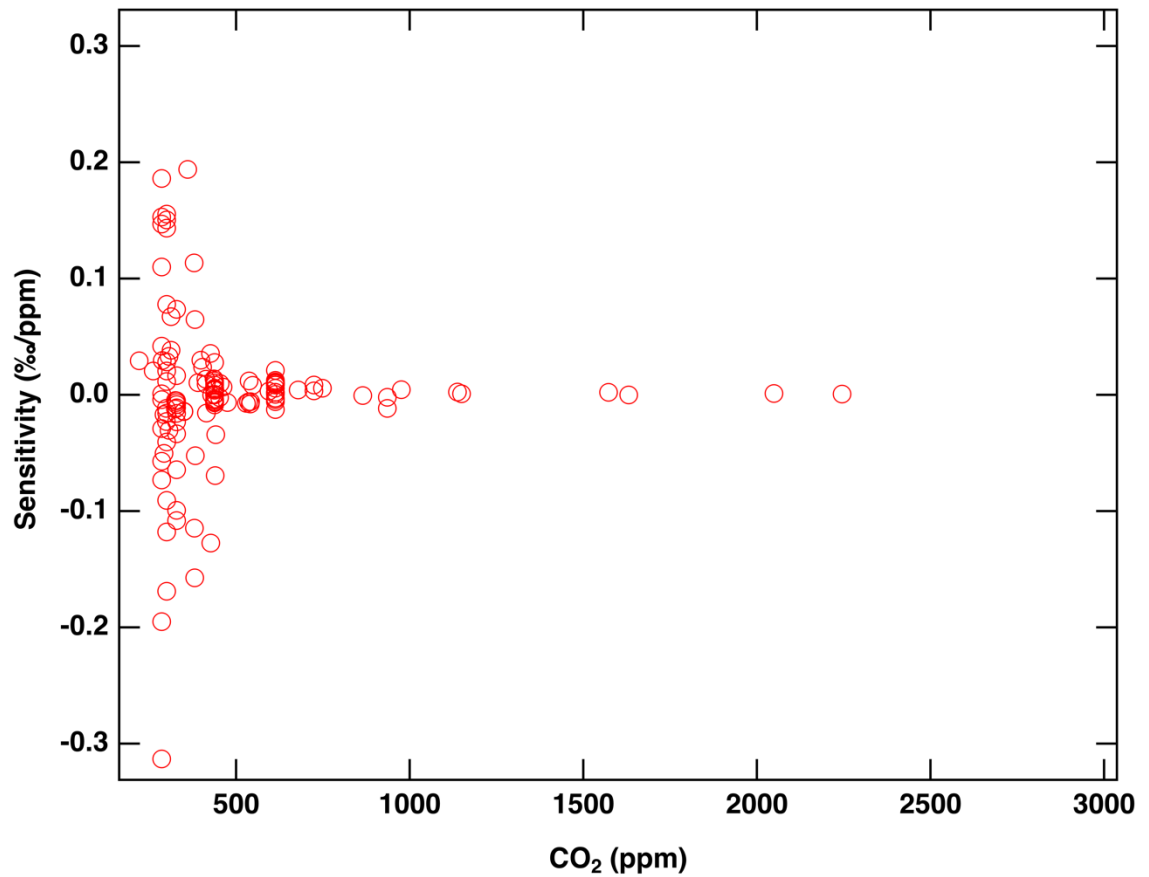


**Figure 33.** Sensitivity values calculated from Van de Water et al. 1994, Penuelas and Estiarte 1997, Feng and Epsetin 1995, Sharma and Williams 2009, Hietz et al. 2005, Saurer et al. 2003, Beerling and Woodward 1995, Penuelas and Azcon-Bieto 1992, Schubert and Jahren 2012, Lomax et al. 2019, Tu et al. 2004, and this study. Studies ranged in  $p\text{CO}_2$  from 270 to 3000 ppm.



### ***Conclusion***

Paleoclimate reconstructions are important to better understand earth systems. By looking at periods (like the PETM) that are analogs to our current situation, we can better predict the direction future climate change. Of particular importance are paleo-CO<sub>2</sub> reconstructions. More paleo-CO<sub>2</sub> proxies are needed to have a clearer picture of past CO<sub>2</sub> levels, especially around periods analogous to our current changing climate, like the PETM.

The C3 plant proxy developed by Schubert and Jahren (2012) is based on a positive hyperbolic relationship between  $\Delta^{13}\text{C}_{\text{leaf}}$  and  $p\text{CO}_2$ . This study of modern *Ginkgo biloba* under elevated CO<sub>2</sub> conditions found a messy but generally opposite relationship: decreasing  $\Delta^{13}\text{C}_{\text{leaf}}$  with  $p\text{CO}_2$ . Several other studies also show differing relationships between  $\Delta^{13}\text{C}_{\text{leaf}}$  and  $p\text{CO}_2$ . Physiological measurements and leaf gas-exchange strategy may be able to explain the range of responses of  $\Delta^{13}\text{C}_{\text{leaf}}$  to  $p\text{CO}_2$ . Without a complete understanding of these influences on  $\Delta^{13}\text{C}_{\text{leaf}}$ , extreme caution should be taken in applying the C3 plant proxy to the fossil record.

### References

- (2020) Earth System Research Laboratory Global Monitoring Division, [www.esrl.noaa.gov](http://www.esrl.noaa.gov).
- Barclay, R.S. and Wing, S.L. (2016) Improving the Ginkgo CO<sub>2</sub> barometer: Implications for the early Cenozoic atmosphere. *Earth and Planetary Science Letters* 439, 158-171.
- Beerling, D.J.t. and Woodward, F.I. (1995) Leaf stable carbon isotope composition records increased water-use efficiency of C<sub>3</sub> plants in response to atmospheric CO<sub>2</sub> enrichment. *Functional Ecology*, 394-401.
- Bender, M.M. (1971) Variations in the <sup>13</sup>C/<sup>12</sup>C ratios of plants in relation to the pathway of photosynthetic carbon dioxide fixation. *Phytochemistry* 10, 1239-1244.
- Berninger, F., Sonninen, E., Aalto, T. and Lloyd, J. (2000) Modeling <sup>13</sup>C discrimination in tree rings. *Global Biogeochemical Cycles* 14, 213-223.
- Bettarini, I., Calderoni, G., Miglietta, F., Raschi, A. and Ehleringer, J. (1995) Isotopic carbon discrimination and leaf nitrogen content of *Erica arborea* L. along a CO<sub>2</sub> concentration gradient in a CO<sub>2</sub> spring in Italy. *Tree Physiology* 15, 327-332.
- Chapman, T., Cui, Y. and Schubert, B. (2019) Stable carbon isotopes of fossil plant lipids support moderately high pCO<sub>2</sub> in the early Paleogene. *ACS Earth and Space Chemistry*.
- Cotton, J.M. and Sheldon, N.D. (2012) New constraints on using paleosols to reconstruct atmospheric pCO<sub>2</sub>. *Geological Society of America Bulletin* 124, 1411-1423.
- Cui, Y., Kump, L.R., Ridgwell, A.J., Charles, A.J., Junium, C.K., Diefendorf, A.F., Freeman, K.H., Urban, N.M. and Harding, I.C. (2011) Slow release of fossil carbon during the Palaeocene–Eocene Thermal Maximum. *Nature Geoscience* 4, 481.
- Cui, Y. and Schubert, B.A. (2016) Quantifying uncertainty of past pCO<sub>2</sub> determined from changes in C<sub>3</sub> plant carbon isotope fractionation. *Geochimica et Cosmochimica Acta* 172, 127-138.
- Cui, Y. and Schubert, B.A. (2017) Atmospheric pCO<sub>2</sub> reconstructed across five early Eocene global warming events. *Earth and Planetary Science Letters* 478, 225-233.
- Diefendorf, A.F., Freeman, K.H. and Wing, S.L. (2012) Distribution and carbon isotope patterns of diterpenoids and triterpenoids in modern temperate C<sub>3</sub> trees and their geochemical significance. *Geochimica et Cosmochimica Acta* 85, 342-356.
- Diefendorf, A.F., Mueller, K.E., Wing, S.L., Koch, P.L. and Freeman, K.H. (2010) Global patterns in leaf <sup>13</sup>C discrimination and implications for studies of past and future climate. *Proceedings of the National Academy of Sciences* 107, 5738-5743.

Ehleringer, J.R. and Cerling, T.E. (1995) Atmospheric CO<sub>2</sub> and the ratio of intercellular to ambient CO<sub>2</sub> concentrations in plants. *Tree physiology* 15, 105-111.

Emiliani, C. (1955) Pleistocene temperatures. *The Journal of Geology* 63, 538-578.

Farquhar, G.D., Ehleringer, J.R. and Hubick, K.T. (1989) Carbon isotope discrimination and photosynthesis. *Annual review of plant biology* 40, 503-537.

Feng, X. and Epstein, S. (1995) Carbon isotopes of trees from arid environments and implications for reconstructing atmospheric CO<sub>2</sub> concentration. *Geochimica et Cosmochimica Acta* 59, 2599-2608.

Fletcher, B.J., Beerling, D.J., Brentnall, S.J. and Royer, D.L. (2005) Fossil bryophytes as recorders of ancient CO<sub>2</sub> levels: experimental evidence and a Cretaceous case study. *Global Biogeochemical Cycles* 19.

Franks, P.J., Royer, D.L., Beerling, D.J., Van de Water, P.K., Cantrill, D.J., Barbour, M.M. and Berry, J.A. (2014) New constraints on atmospheric CO<sub>2</sub> concentration for the Phanerozoic. *Geophysical Research Letters* 41, 4685-4694.

Freeman, K.H. and Hayes, J.M. (1992) Fractionation of carbon isotopes by phytoplankton and estimates of ancient CO<sub>2</sub> levels. *Global biogeochemical cycles* 6, 185-198.

Friend, A.D., Woodward, F.I. and Switsur, V.R. (1989) Field measurements of photosynthesis, stomatal conductance, leaf nitrogen and  $\delta^{13}\text{C}$  along altitudinal gradients in Scotland. *Functional Ecology*, 117-122.

Hietz, P., Wanek, W. and Dünisch, O. (2005) Long-term trends in cellulose  $\delta^{13}\text{C}$  and water-use efficiency of tropical *Cedrela* and *Swietenia* from Brazil. *Tree physiology* 25, 745-752.

Hyland, E.G. and Sheldon, N.D. (2013) Coupled CO<sub>2</sub>-climate response during the early Eocene climatic optimum. *Palaeogeography, Palaeoclimatology, Palaeoecology* 369, 125-135.

IPCC, 2013: *Climate Change 2013: The Physical Science Basis. Contribution of Working Group I to the Fifth Assessment Report of the Intergovernmental Panel on Climate Change* [Stocker, T.F., D. Qin, G.-K. Plattner, M. Tignor, S.K. Allen, J. Boschung, A. Nauels, Y. Xia, V. Bex and P.M. Midgley (eds.)]. Cambridge University Press, Cambridge, United Kingdom and New York, NY, USA, 1535 pp.

IPCC, 2014: *Climate Change 2014: Synthesis Report. Contribution of Working Groups I, II and III to the Fifth Assessment Report of the Intergovernmental Panel on Climate Change* [Core Writing Team, R.K. Pachauri and L.A. Meyer (eds.)]. IPCC, Geneva, Switzerland, 151 pp.

IPCC, 2018: Summary for Policymakers. In: *Global Warming of 1.5°C. An IPCC Special Report on the impacts of global warming of 1.5°C above pre-industrial levels and related global greenhouse gas emission pathways, in the context of strengthening the global response to the threat of climate change, sustainable development, and efforts to eradicate poverty* [Masson-Delmotte, V., P. Zhai, H.-O. Pörtner, D. Roberts, J. Skea, P.R. Shukla, A. Pirani, W. Moufouma-Okia, C. Péan, R. Pidcock, S. Connors, J.B.R. Matthews, Y. Chen, X. Zhou, M.I. Gomis, E. Lonnoy, T. Maycock, M. Tignor, and T. Waterfield (eds.)]. In Press.

Jagniecki, E.A., Lowenstein, T.K., Jenkins, D.M. and Demicco, R.V. (2015) Eocene atmospheric CO<sub>2</sub> from the nahcolite proxy. *Geology* 43, 1075-1078.  
Klochko, K., Kaufman, A.J., Yao, W., Byrne, R.H. and Tossell, J.A. (2006) Experimental measurement of boron isotope fractionation in seawater. *Earth and Planetary Science Letters* 248, 276-285.

Kohn, M.J. (2016) Carbon isotope discrimination in C<sub>3</sub> land plants is independent of natural variations in pCO<sub>2</sub>. *Geochemical Perspectives Letters* 2, 35-43.

Kraus, M.J., McInerney, F.A., Wing, S.L., Secord, R., Baczynski, A.A. and Bloch, J.I. (2013) Paleohydrologic response to continental warming during the Paleocene–Eocene thermal maximum, Bighorn Basin, Wyoming. *Palaeogeography, Palaeoclimatology, Palaeoecology* 370, 196-208.

Kürschner, W.M., van der Burgh, J., Visscher, H. and Dilcher, D.L. (1996) Oak leaves as biosensors of late Neogene and early Pleistocene paleoatmospheric CO<sub>2</sub> concentrations. *Marine Micropaleontology* 27, 299-312.

Lloyd, J. and Farquhar, G.D. (1994) <sup>13</sup>C discrimination during CO<sub>2</sub> assimilation by the terrestrial biosphere. *Oecologia* 99, 201-215.

Lomax, B.H., Lake, J.A., Leng, M.J. and Jardine, P.E. (2019) An experimental evaluation of the use of Δ<sup>13</sup>C as a proxy for palaeoatmospheric CO<sub>2</sub>. *Geochimica et Cosmochimica Acta* 247, 162-174.

Lüthi, D., Le Floch, M., Bereiter, B., Blunier, T., Barnola, J.-M., Siegenthaler, U., Raynaud, D., Jouzel, J., Fischer, H. and Kawamura, K. (2008) High-resolution carbon dioxide concentration record 650,000–800,000 years before present. *Nature* 453, 379-382.

Marchitto, T.M., Curry, W.B., Lynch-Stieglitz, J., Bryan, S.P., Cobb, K.M. and Lund, D.C. (2014) Improved oxygen isotope temperature calibrations for cosmopolitan benthic foraminifera. *Geochimica et Cosmochimica Acta* 130, 1-11.

McInerney, F.A. and Wing, S.L. (2011) The Paleocene-Eocene Thermal Maximum: A perturbation of carbon cycle, climate, and biosphere with implications for the future. *Annual Review of Earth and Planetary Sciences* 39, 489-516.

- O'Leary, M.H. (1988) Carbon isotopes in photosynthesis. *Bioscience* 38, 328-336.
- Panchuk, K., Ridgwell, A. and Kump, L.R. (2008) Sedimentary response to Paleocene-Eocene Thermal Maximum carbon release: A model-data comparison. *Geology* 36, 315-318.
- Peñuelas, J. and Azcón-Bieto, J. (1992) Changes in leaf  $\Delta^{13}\text{C}$  of herbarium plant species during the last 3 centuries of  $\text{CO}_2$  increase. *Plant, Cell & Environment* 15, 485-489.
- Peñuelas, J. and Estiarte, M. (1996) Trends in plant carbon concentration and plant demand for N throughout this century. *Oecologia* 109, 69-73.
- Porter, A.S., Gerald, C.E.-F., Yiotis, C., Montañez, I.P. and McElwain, J.C. (2019) Testing the accuracy of new paleoatmospheric  $\text{CO}_2$  proxies based on plant stable carbon isotopic composition and stomatal traits in a range of simulated paleoatmospheric  $\text{O}_2$ :  $\text{CO}_2$  ratios. *Geochimica et Cosmochimica Acta*.
- Royer, D.L. (2001) Stomatal density and stomatal index as indicators of paleoatmospheric  $\text{CO}_2$  concentration. *Review of Palaeobotany and Palynology* 114, 1-28.
- Royer, D.L., Moynihan, K.M., McKee, M.L., Londoño, L. and Franks, P.J. (2019) Sensitivity of a leaf gas-exchange model for estimating paleoatmospheric  $\text{CO}_2$  concentration. *Climate of the Past* 15, 795-809.
- Saurer, M., Cherubini, P., Bonani, G. and Siegwolf, R. (2003) Tracing carbon uptake from a natural  $\text{CO}_2$  spring into tree rings: an isotope approach. *Tree Physiology* 23, 997-1004.
- Schubert, B.A. and Jahren, A.H. (2012) The effect of atmospheric  $\text{CO}_2$  concentration on carbon isotope fractionation in  $\text{C}_3$  land plants. *Geochimica et Cosmochimica Acta* 96, 29-43.
- Schubert, B.A. and Jahren, A.H. (2015) Global increase in plant carbon isotope fractionation following the Last Glacial Maximum caused by increase in atmospheric  $\text{CO}_2$ . *Geology* 43, 435-438.
- Sharma, S. and Williams, D.G. (2009) Carbon and oxygen isotope analysis of leaf biomass reveals contrasting photosynthetic responses to elevated  $\text{CO}_2$  near geologic vents in Yellowstone National Park. *Biogeosciences* 6, 25-31.
- Tcherkez, G.G.B., Farquhar, G.D. and Andrews, T.J. (2006) Despite slow catalysis and confused substrate specificity, all ribulose biphosphate carboxylases may be nearly perfectly optimized. *Proceedings of the National Academy of Sciences* 103, 7246-7251.
- Tralau, H. (1968) Evolutionary trends in the genus *Ginkgo*. *Lethaia* 1, 63-101.

Treydte, K.S., Frank, D.C., Saurer, M., Helle, G., Schleser, G.H. and Esper, J. (2009) Impact of climate and CO<sub>2</sub> on a millennium-long tree-ring carbon isotope record. *Geochimica et Cosmochimica Acta* 73, 4635-4647.

Tu, T.T.N., Kürschner, W.M., Schouten, S. and Van Bergen, P.F. (2004) Leaf carbon isotope composition of fossil and extant oaks grown under differing atmospheric CO<sub>2</sub> levels. *Palaeogeography, Palaeoclimatology, Palaeoecology* 212, 199-213.

Van de Water, P.K., Leavitt, S.W. and Betancourt, J.L. (1994) Trends in stomatal density and <sup>13</sup>C/<sup>12</sup>C ratios of *Pinus flexilis* needles during last glacial-interglacial cycle. *Science* 264, 239-243.

Voelker, S.L., Brooks, J.R., Meinzer, F.C., Anderson, R., Bader, M.K.F., Battipaglia, G., Becklin, K.M., Beerling, D., Bert, D. and Betancourt, J.L. (2016) A dynamic leaf gas-exchange strategy is conserved in woody plants under changing ambient CO<sub>2</sub>: evidence from carbon isotope discrimination in paleo and CO<sub>2</sub> enrichment studies. *Global Change Biology* 22, 889-902.

Wang, W., Liu, X., Shao, X., Leavitt, S., Xu, G., An, W. and Qin, D. (2011) A 200 year temperature record from tree ring  $\delta^{13}\text{C}$  at the Qaidam Basin of the Tibetan Plateau after identifying the optimum method to correct for changing atmospheric CO<sub>2</sub> and  $\delta^{13}\text{C}$ . *Journal of Geophysical Research: Biogeosciences* 116.

Westerhold, T., Röhl, U., Donner, B. and Zachos, J.C. (2018) Global extent of early Eocene hyperthermal events: A new Pacific benthic foraminiferal isotope record from Shatsky Rise (ODP Site 1209). *Paleoceanography and Paleoclimatology* 33, 626-642.

Wing, S.L. and Currano, E.D. (2013) Plant response to a global greenhouse event 56 million years ago. *American Journal of Botany* 100, 1234-1254.

Wong, C.I. and Breecker, D.O. (2015) Advancements in the use of speleothems as climate archives. *Quaternary Science Reviews* 127, 1-18.

Zeebe, R.E. (2005) Stable boron isotope fractionation between dissolved B (OH)<sup>3</sup> and B (OH)<sup>4-</sup>. *Geochimica et Cosmochimica Acta* 69, 2753-2766.

Zeebe, R.E., Zachos, J.C. and Dickens, G.R. (2009) Carbon dioxide forcing alone insufficient to explain Palaeocene–Eocene Thermal Maximum warming. *Nature Geoscience* 2, 576-580.

Zhou, Z. and Zheng, S. (2003) The missing link in Ginkgo evolution. *Nature* 423, 821-822.